Palaeogeography, Palaeoclimatology, Palaeoecology 492 (2018) 104–125

Contents lists available at ScienceDirect

Palaeogeography, Palaeoclimatology, Palaeoecology

journal homepage: www.elsevier.com/locate/palaeo

Geochemistry of heavy minerals and U–Pb detrital zircon geochronology in the Manantiales Basin: Implications for Frontal Cordillera uplift and foreland basin connectivity in the Andes of central Argentina

Luisa Pinto[a,*], Pablo Alarcón[b,f,g], Andrew Morton[c,d], Maximiliano Naipauer[e]

[a] Departamento de Geología, FCFM, Universidad de Chile, Plaza Ercilla 803, Casilla 13518, Correo 21, Santiago, Chile
[b] Universidad de Concepción, Facultad de Ciencias Químicas, Departamento Ciencias de la Tierra, Edmundo Larenas 129, Casilla 160-C, Concepción, Chile
[c] HM Research Associates, Giddanmu, St Ishmaels, Haverfordwest SA62 3TJ, UK
[d] CASP, University of Cambridge, Cambridge CB3 0DH, UK
[e] Instituto de Estudios Andinos Don Pablo Groeber (UBA–CONICET), Intendente Güiraldes 2160, Ciudad Universitaria, Pabellón II, Codigo Postal 1428 Buenos Aires, Argentina
[f] Facultad de Ciencias, Universidad Austral de Chile, Av. Rector Eduardo Morales Miranda 23, Valdivia, Chile
[g] G2O Ltda, Consultoría Geológica e Hidrogeológica, San Ignacio 879, Puerto Varas, Chile

ARTICLE INFO

Keywords:
Miocene
Provenance
Clinopyroxene
Amphibole
La Ramada

ABSTRACT

The Manantiales Foreland Basin, located at ~32°15′S in the Frontal Cordillera, Argentina, contains the sedimentary record of erosion of igneous basement and Miocene volcanic rocks exhumed during the Andean orogeny. U–Pb ages of detrital zircons from the basin fill succession (Chinches Formation) constrain the onset of deposition to ca. 22 Ma (early Miocene). We present the first geochronological control (ca. 22 Ma) from the lower part of the Manantiales Foreland Basin (Areniscas Chocolate member) on the basis of U–Pb ages of detrital zircons, shedding light about an older initiation of this foreland basin. The main heavy mineral association in the sedimentary basin, clinopyroxene + amphibole, indicates two events of volcanic supply, probably corresponding to the Farellones Formation in the Principal Cordillera, and the La Ramada Volcanic Complex and subvolcanic rocks similar to the La Laguna body in the Argentinean Frontal Cordillera. Detrital zircon geochronology indicates dominant sourcing from upper Paleozoic–lower Triassic Choiyoi Magmatic Province rocks. Initial sediment supply at ca. 22–19 Ma was from the Cenozoic volcanic arc of the Principal Cordillera. At ca. 19 Ma, exhumation of the Frontal Cordillera was registered by supply from the Choiyoi Magmatic Province, related to tectonic uplift of a western block (La Ramada–El Espinacito ranges) through a thrust of the La Ramada fold-and-thrust belt. At ca. 16 Ma, supply from the Cenozoic volcanic arc recommenced, providing evidence for capture and erosion of the Principal Cordillera, which could be related to thrusting in normal sequence of the La Ramada fold-and-thrust belt. At ca. 10 Ma, the La Ramada Volcanic Complex and rocks similar to the La Laguna subvolcanic body became a local source of sediment for the basin. The Manantiales Foreland Basin was linked to Neogene sedimentary basins in the Precordillera at its first part in its history, between ca. 22 and 19 Ma and probably until ca. 12 Ma, when the eastern Frontal Cordillera (Cordillera del Tigre) and Precordillera were uplifted, and the foreland basin was broken. Thus, the Frontal Cordillera was uplifted through two diachronous thick-skinned blocks from west (La Ramada–El Espinacito ranges) to east (Cordillera del Tigre). This result can explain the diverse ages for uplift deduced for the Frontal Cordillera in previous studies, where it has been considered rather as a singular N-S block. The source of late Mesoproterozoic detrital zircons registered in the Manantiales Basin is uncertain, but we infer recycling from Mesozoic sedimentary rocks of the Principal Cordillera.

1. Introduction

The variable deformational and exhumation regime along strike of the Andean orogenic belt has profound effects on the development of its linked basins and depocenters, i.e., controlling subsidence, initiation and style of sedimentation and long-term paleogeographic evolution in terms of paleodrainage system. The foreland basins of the central and southern-central Andes are a clear example of the complexity of the

* Corresponding author.
E-mail address: lpinto@ing.uchile.cl (L. Pinto).

https://doi.org/10.1016/j.palaeo.2017.12.017
Received 24 November 2016; Received in revised form 16 December 2017; Accepted 16 December 2017
Available online 21 December 2017
0031-0182/

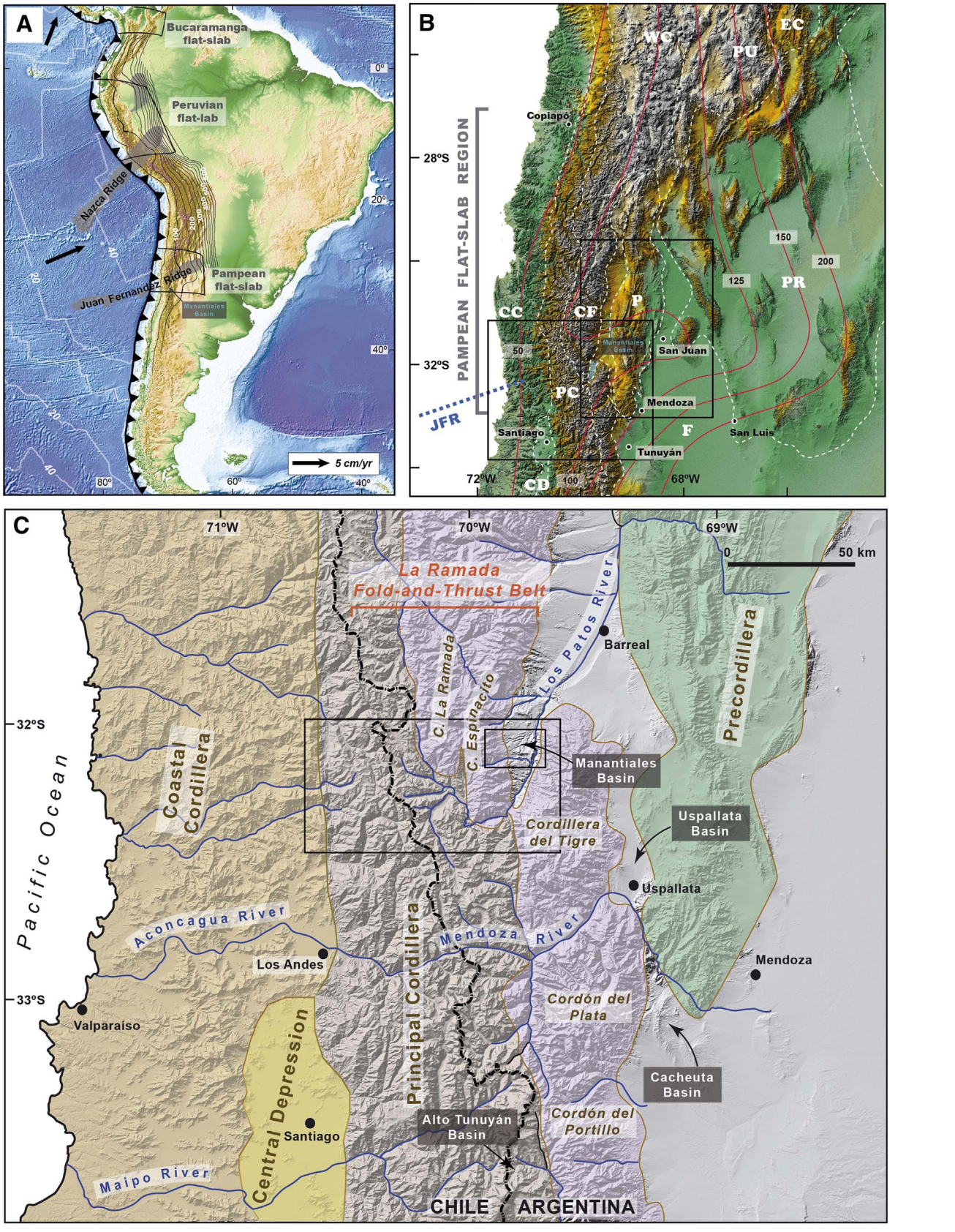

(caption on next page)

orogenic evolution, revealing differences in timing of exhumation and advance of the deformation front. In the southern part of the Puna, northern Argentina (~24°–28°S, Fig. 1A–B), initiation of foreland basins has been interpreted as Paleogene (Jordan et al., 1983; Carrapa et al., 2011, 2012). Further south (~28°–32°S, Fig. 1A–B), the beginning of contractional deformation is likely to be as early as early

Fig. 1. (A) Geological setting of South America with depth contours of slab indicated by thin black lines, and subducting oceanic plateaus in translucent gray (modified from Hu et al., 2016, and based on Hayes et al., 2012). The major flat-slabs in South America are outlined with thick black lines. The locations of oceanic plateaus and flat slabs are modified from Gutscher et al. (2000) and Ramos and Folguera (2009). Location of the Manantiales Basin is indicated. (B) Main morphostructural domains in the Pampean flat-slab segment of the Andes (dashed white lines), with depth contours of slab indicated (red lines). *Abbreviations*: CC, Coastal Cordillera; CD, Central Depression; EC, Eastern Cordillera; FC, Frontal Cordillera; P, Precordillera; PC, Principal Cordillera; PR, Pampean Ranges; PU, Puna; WC, Western Cordillera (based on Rivano et al., 1993; Jordan et al., 1996; Ramos et al., 2002; Gans et al., 2011; Carrapa et al., 2011; Levina et al., 2014; Hoke et al., 2014; Alarcón and Pinto, 2015). JFR, Juan Fernández Ridge (location in dashed blue line). Lower left and upper right boxes indicate area covered by Figs. 1C and 2, respectively. Location of the Manantiales Basin is indicated, and some cities are labeled with black dots for reference. (C) Regional scale DEM with tectonic and morphological global features, showing location of the study area (modified from Alarcón and Pinto, 2015). Morphostructural units are delimited and remarked by translucent colors. The location of the main Neogene foreland basins (based on Irigoyen et al., 2000; Hoke et al., 2014; Mahoney et al., 2014; Giambiagi et al., 2016) and location of subranges in the Frontal Cordillera (pink colour) are also indicated. Some cities are labeled with black dots for reference. Large and small boxes indicate areas covered by Figs. 2 and 6, respectively. (For interpretation of the references to colour in this figure legend, the reader is referred to the web version of this article.)

Cenozoic and onset of foreland basin occurs in the Eocene (Fosdick et al., 2017). In contrast, the northernmost exposure of the Neuquén Basin (34°–36°S) records a Late Cretaceous initiation for foreland sedimentation (Balgord and Carrapa, 2016). Interestingly, between 31°S and 33°S, there are a number of N-S elongated depocenters (including Manantiales, Alto Tunuyán, Talacasto, Pachaco, Las Peñas, Uspallata, Albarracín and Riquiliponche) that correspond to Neogene foreland basins (Figs. 1C and 2) (e.g., Giambiagi et al., 2003; Levina et al., 2014; Porras et al., 2016). The initiation of these foreland basins is still not fully constrained.

The relationship of connectivity and paleogeographic evolution among the latter basins and further with the Bermejo foreland basin (Fig. 2A) has been a matter of ongoing debate, concerning whether the Neogene basin fills fit the continuous foreland basin style (Levina et al., 2014; Fosdick et al., 2017) or correspond to a piggyback or intermontane basin on top of an active thrust belt (Hoke et al., 2014, 2015). An alternative model suggests this basin evolved as a broken foreland basin (Hoke et al., 2015) akin the Sierras Pampeanas broken foreland (Jordan, 1995; Ramos et al., 2002) in response to an eastward-propagated thick-skinned deformation front.

For latitudes between 27° and 33.5°S, Ramos et al. (2002) and Giambiagi et al. (2003) proposed a Miocene to Pliocene migration of the deformation front from west to east, i.e., from the Cordillera Principal to the Pampean Ranges (Fig. 1B), together with diachronous uplift of Andean ranges from north to south, in response to the southward migration of a flat-slab subduction (e.g., Yáñez et al., 2001; Ramos et al., 2002; Martinod et al., 2010). However, the supposed uplift of the Cordillera Principal (ca. 20–9 Ma), the Frontal Cordillera (ca. 10–3 Ma) and Precordillera (post–4 Ma), associated with the development of the Pampean flat-slab (e.g., Ramos, 1999a; Ramos et al., 2002) and the southward migration of the uplift has been recently challenged by the existence of a pre-Miocene paleo-topography in the Frontal Cordillera and the Precordillera (e.g., Walcek and Hoke, 2012; Hoke et al., 2015; Fosdick et al., 2017) and a nearly synchronous onset of shortening along strike of the Precordillera (Suriano et al., 2017).

In this context, the Miocene Manantiales Foreland Basin (MFB) stands out as a crucial piece to understand first Andean tectonic events at these latitudes (~32°15′S). Its genesis is linked to the Principal Cordillera and the Frontal Cordillera (Jordan et al., 1996; Cristallini and Ramos, 2000), and therefore allows us extract the tectonic history of the southern-central Andean cordilleran system. Accordingly, in this paper we present an integrated analysis of the depositional systems, tectonic control, geochronology (Maximum Depositional Ages) and provenance of the MFB (32°–32.5°S, Figs. 1, 2 and 3), combining geochemistry of heavy minerals, and detrital zircon U–Pb geochronology. The key westernmost location, and the thick > 3 km stratigraphic succession there exposed (Jordan et al., 1996) offers a unique opportunity to address the two-fold purpose of this study: a) to constrain the timing of exhumation and unroofing events of the Principal and Frontal Cordilleras at ~32°15′S associated with thrusting of an Andean fold-and-thrust belt; b) to interpret the paleogeographic evolution of this region and shed light about regional correlations with other Neogene basins either in terms of a foreland basin system (DeCelles and Giles, 1996) or isolated depocenters.

2. Geological setting

The MFB is located within the Frontal Cordillera between 32° and 32.5°S (Figs. 1, 2 and 3), and filled with > 3 km of sedimentary rocks (Jordan et al., 1996). Previous authors (e.g., Ramos, 1999a) included the MFB as part of the Iglesia–Calingasta basins, which are located between the Frontal Cordillera and the Precordillera (Fig. 2). However, the MFB can be differentiated from the Iglesia–Uspallata basins because of its morphotectonic setting (completely within the Frontal Cordillera), an older history (early Miocene) for its development (Jordan et al., 1996; Pérez, 2001; López et al., 2011; Hoke et al., 2014), and because it has a stratigraphic architecture of a foredeep proximal basin (e.g., Pérez, 1995, 2001; Jordan et al., 1996). The MFB is associated with the eastward propagation of the La Ramada fold-and-thrust belt (Pérez, 1995, 2001; Jordan et al., 1996; Cristallini and Ramos, 2000; Hoke et al., 2014). Today, the MFB appears as an intermontane basin, bounded by the Cordón del Espinacito and the Cordillera del Tigre (Jordan et al., 1996; Cristallini et al., 1996), both included within the Frontal Cordillera (Figs. 1C, 3A and B). We have to clarify that Cristallini and Ramos (2000) defined the eastern border of the La Ramada fold-and-thrust belt as the limit between the Principal Cordillera and Frontal Cordillera; however, the limit between these two ranges is ambiguous. We considered this limit as the west border of the Choiyoi Magmatic Province (Fig. 3B) according to Hoke et al. (2014).

The La Ramada fold-and-thrust belt is located in the southern region of the Pampean flat-slab segment (Figs. 1A, C and 3) and developed as an expression of Neogene contractional tectonics (Cristallini and Ramos, 2000). This fold-and-thrust belt is an east-vergent thick- and thin-skinned structural system, in which the Permo–Triassic magmatic province (Choiyoi Group) and the Meso-Cenozoic sedimentary and volcanic covers (Fig. 3) were deformed (e.g., Cristallini and Ramos, 2000; Ramos et al., 2002). The tectonic history of the Principal Cordillera and Frontal Cordillera is recorded by deformation within the fold-and-thrust belt and the related syntectonic volcano-sedimentary basins (e.g., Jordan et al., 1993; Giambiagi et al., 2016; Suriano et al., 2017) (Fig. 2).

The Principal Cordillera is a range formed by Meso-Cenozoic rocks underlain by basement rocks, which probably correspond to the Choiyoi Magmatic Province (Fig. 3) (e.g., Cristallini et al., 1994). It is ~800 km long (~30°–37°S, Ramos, 1999b) and ~50 km wide (Fig. 3B). Initial uplift and associated deformation within this range would have been produced by the tectonic inversion of the Abanico Basin from the Oligo–Miocene (~23–21 Ma, Fig. 3) (e.g., Charrier et al., 2002, 2007; Muñoz-Sáez et al., 2014, and references therein). The eastern part of the Principal Cordillera corresponds to the innermost thin-skinned tectonic block of the La Ramada fold-and-thrust belt (Fig. 3B). On the other hand, the Frontal Cordillera is a range mainly composed of rocks of the Choiyoi Magmatic Province, and where the Cenozoic cover is almost absent (Fig. 3B). The proposed structural models indicate that this range corresponds to mainly thick-skinned blocks of the La Ramada fold-and-thrust belt and would have developed after the Principal Cordillera (e.g., Cristallini and Ramos, 2000), producing a minimal shortening of ~18 km (Giambiagi et al., 2016). Although recent geomorphological data (Hoke et al., 2015) suggest that

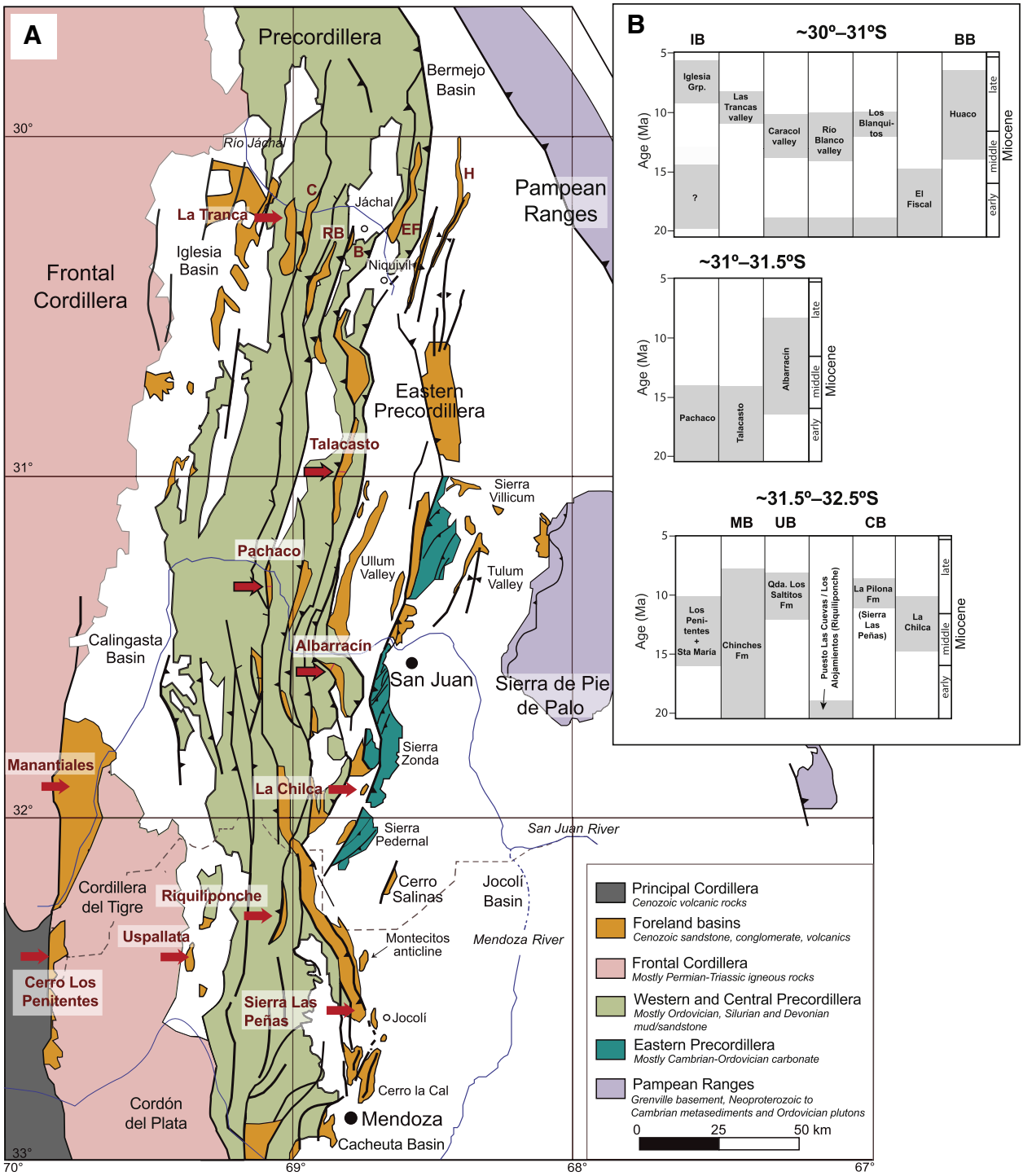

Fig. 2. (A) Location of sedimentary basin deposits within the Andean morphostructural domains (modified from Vergés et al., 2007, and Levina et al., 2014). The covered area is shown in Fig. 1B. *Abbreviations*: B, Los Blanquitos, C, Caracol valley; EF, El Fiscal; H, Huaco; RB, Río Blanco valley. (B) Correlation between the Miocene syntectonic sedimentary sequences on the Pampean flat-slab region (based on Jordan et al., 1993, 1996; Bercowski et al., 1993; Vicente, 2005; Reyna et al., 2010; Iverson et al., 2012; Levina et al., 2014; Hoke et al., 2014; Suriano et al., 2017). The gray areas indicate the approximate age of stratigraphic sequences in the Andean basins. When a sequence belongs to a defined basin it is indicated (BB, Bermejo Foreland Basin; CB, Cacheuta Basin; IB, Iglesia Basin; MB, Manantiales Basin; UB, Uspallata Basin).

the Frontal Cordillera started to form < 25 Ma, the authors did not integrate the available tectono-stratigraphic information associated with the history of this mountain range.

3. Stratigraphy of the Manantiales Foreland Basin

The filling of the MFB is represented by the Miocene Chinches Formation (Figs. 1C and 3), which is ~3600 m thick (Jordan et al., 1996) and is composed of sedimentary and volcanic material. The succession, which is ascribed to the Chinches Formation, was subdivided into three main members by Mirré (1966):

First, the Areniscas Chocolate member, which corresponds to the lowest part of the sedimentary succession, is composed of ~40 m to ~350 m of brown and green sandstones, with scarce conglomerates (Mirré, 1966; Pérez, 2001). The sandstones, which show cross-stratification, were interpreted as eolian deposits (Pérez, 2001). A lower

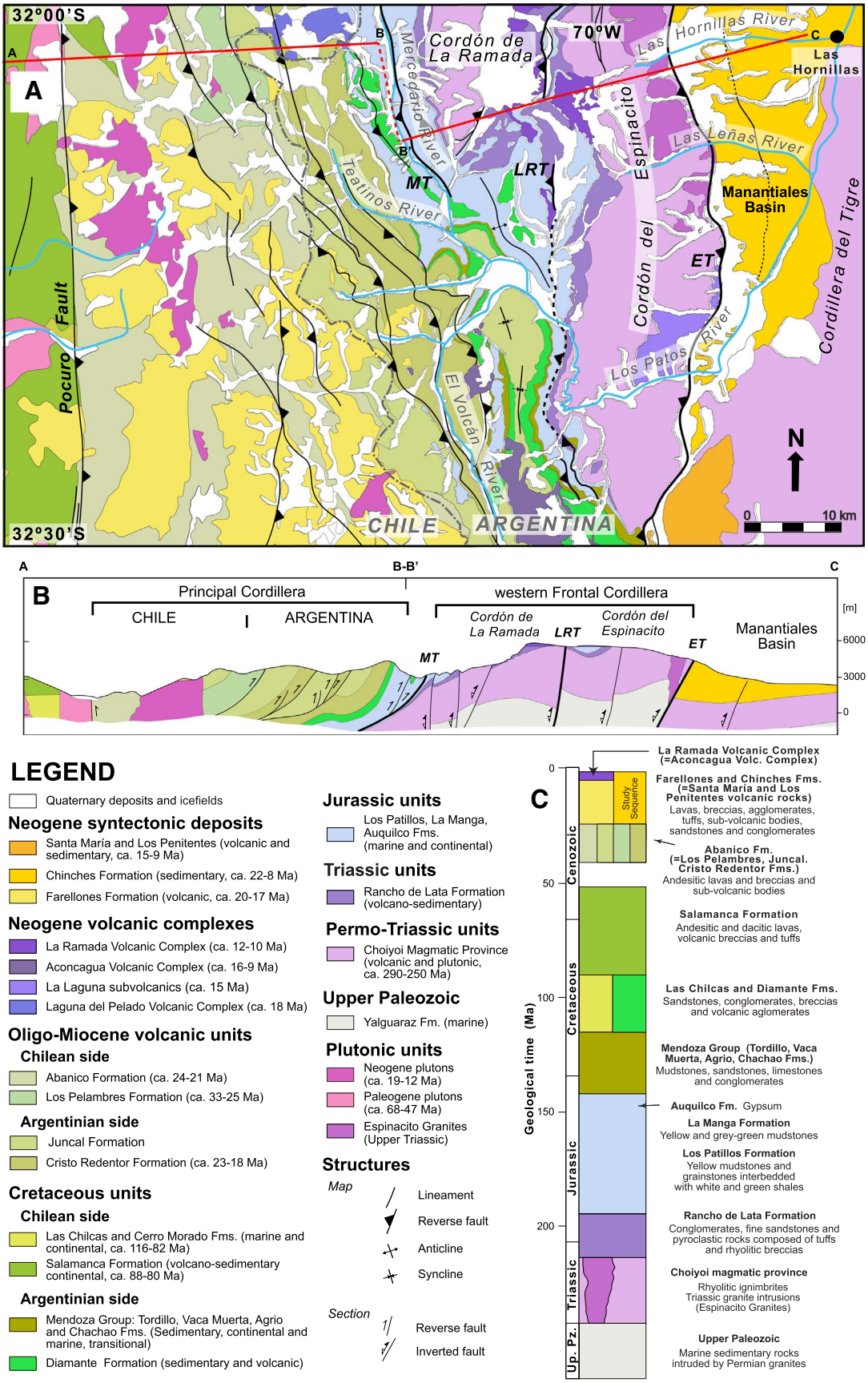

Fig. 3. (A) Geological map, (B) section, and (C) generalized stratigraphic column for the studied region modified from Alarcón and Pinto (2015) and based on Rivano et al. (1993), Cristallini and Cangini (1993), Cristallini et al. (1996), Pérez (1995, 2001), Jordan et al. (1996), Ramos, V., et al. (1996), Ramos, V.A., et al. (1996), Cristallini and Ramos (2000), Sernageomin (2003), Vicente (2005), Charrier et al. (2007), Mpodozis et al. (2009), Jara and Charrier (2014) and Boyce (2015). The studied sequence (Chinches Formation) is indicated in Fig. 3C. The main thrusts of the La Ramada fold-and-thrust belt, discussed in the text, are shown in the map and section: MT, Mercedario Thrust, LRT, La Ramada Thrust, and ET, El Espinacito Thrust.

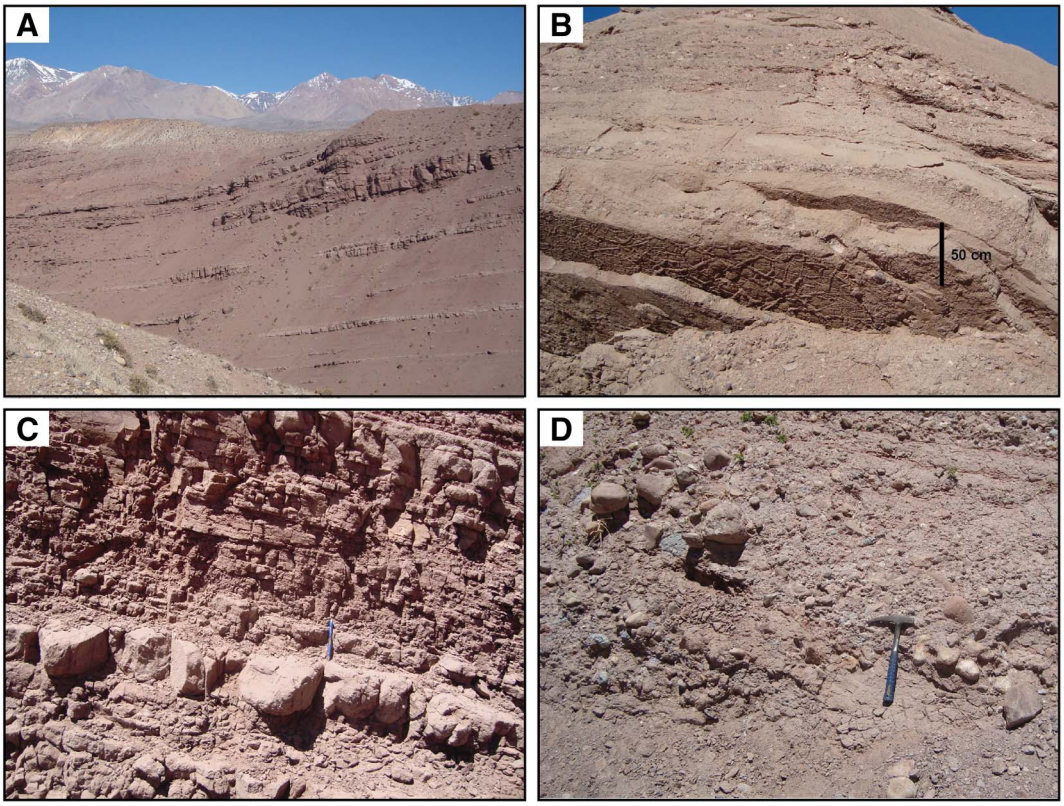

Fig. 4. Photographs of the Chinches Formation outcrops: (A) Aldeco River, NW view. Strata dip to the west; (B) Sandstones and conglomerates in the lower Chinches Formation close to Las Hornillas; (C) Fine-grained facies in the lower Chinches Formation close to Las Hornillas; (D) Coarse-grained facies in the upper Chinches Formation close to San Juan Refuge. Localities and rivers are shown in Fig. 6.

Miocene age was assigned to this member by Pérez (1995), but geochronological constraints are currently lacking.

Second, the Las Hornillas volcanic breccia member, which overlies the Areniscas Chocolate member at Las Hornillas (Figs. 3A and 6). This breccia has been correlated with the Las Pichireguas andesitic breccia outcropping at the base of the La Ramada Vocanic Complex in the Cordón de La Ramada (Fig. 3), and represents the distal volcanic facies of the Farellones Formation (Pérez, 1995). The Las Hornillas volcanic breccia member is classified as a trachyandesite (Alarcón and Pinto, 2015), with similar geochemistry to that of the middle Miocene La Laguna subvolcanic body (Pérez and Ramos, 1996). Pérez (1995, 2001) correlates the Las Hornillas volcanic breccia member with the subvolcanic hornblende-bearing andesites outcropping in Barreal (Fig. 1C). The Barreal andesites have an age of 20.1 ± 2.5 Ma (K–Ar, whole-rock, Leveratto, 1976), and hence, a ca. 20 Ma age can be estimated for the Las Hornillas volcanic breccia member.

Third, the Conglomeratic Sandstones member, which overlie the Las Hornillas volcanic breccia member, forms the majority of the MFB fill. The member consists of clastic sedimentary rocks ranging from shales to conglomerates, interbedded with volcanic rocks (Figs. 4 and 5) (Jordan et al., 1996; Pérez, 2001). Deposition took place mainly in braided fluvial channel and floodplain environments, with alluvial fan sedimentary rocks towards the top and with paleocurrent directions oriented from west to east (Jordan et al., 1996). Three fossiliferous lacustrine deposits have been recognized within the succession, and are believed to be related to tectonic activation of thrusts of the La Ramada fold-and-thrust belt (Jordan et al., 1996). One of the lacustrine deposits (~2500 m, Fig. 5) has been interpreted as evidence of a marine transgression based on microfossils (Pérez and Ramos, 1996; Pérez, 2001). However, the association of sedimentary facies (Jordan et al., 1996) and ratios of stable isotopes of carbon and oxygen do not support such a transgression (Ruskin et al., 2011).

Previous provenance and geochronological studies of the Chinches Formation involved paleocurrent analyses, petrography, zircon fission-track ages, magnetostratigraphy, paleontology, geochemistry of sandstones and conglomerate clast counts (Iglesia Llanos, 1995; Pérez, 1995, 2001; Pérez and Ramos, 1996; López et al., 2011; Jordan et al., 1996; Alarcón and Pinto, 2015). Paleocurrent data indicate that the source rocks were mainly located to the west of the MFB (Jordan et al., 1996), in the Principal Cordillera and Frontal Cordillera (Fig. 5). Provenance studies in the basin (e.g., Mirré, 1966; Jordan et al., 1996; Pérez, 2001; Alarcón and Pinto, 2015) indicate derivation from the Choiyoi Group, Mesozoic sedimentary and Cenozoic volcanic rocks (Figs. 3 and 5). However, uncertainties about which volcanic units were uplifted and eroded still remain. Potential Cenozoic volcanic source rocks include the Oligo-Miocene volcanic and subvolcanic units (ca. 24–17 Ma, Rivano et al., 1990, 1993; Ramos et al., 1991; Cristallini and Cangini, 1993; Mpodozis et al., 2009; Jara and Charrier, 2014) in the Principal Cordillera, together with the Miocene volcanic and subvolcanic units (ca. 15–11 Ma, Pérez, 1995; Pérez and Ramos, 1996) in the Frontal Cordillera (Fig. 3). Variations in provenance led Alarcón and Pinto (2015) to subdivide the succession into three informal stratigraphic units (lower, middle and upper). The relationship between the provenance-based subdivision and the lithostratigraphic subdivision of Mirré (1966) is shown in Fig. 5.

Furthermore, the available controls (fission track thermochronology, magnetostratigraphy, paleontology) have established an early to middle Miocene age for the majority of the MFB fill (Jordan et al., 1996; Pérez, 2001; López et al., 2011; Ruskin et al., 2011). However, more geochronological constraints on the onset of deposition are needed to establish the precise tectonic significance of the MFB given its close relationship with the La Ramada fold-and-thrust belt, and because it is representative of syntectonic basins in the Frontal Cordillera at ~32°–32.5°S.

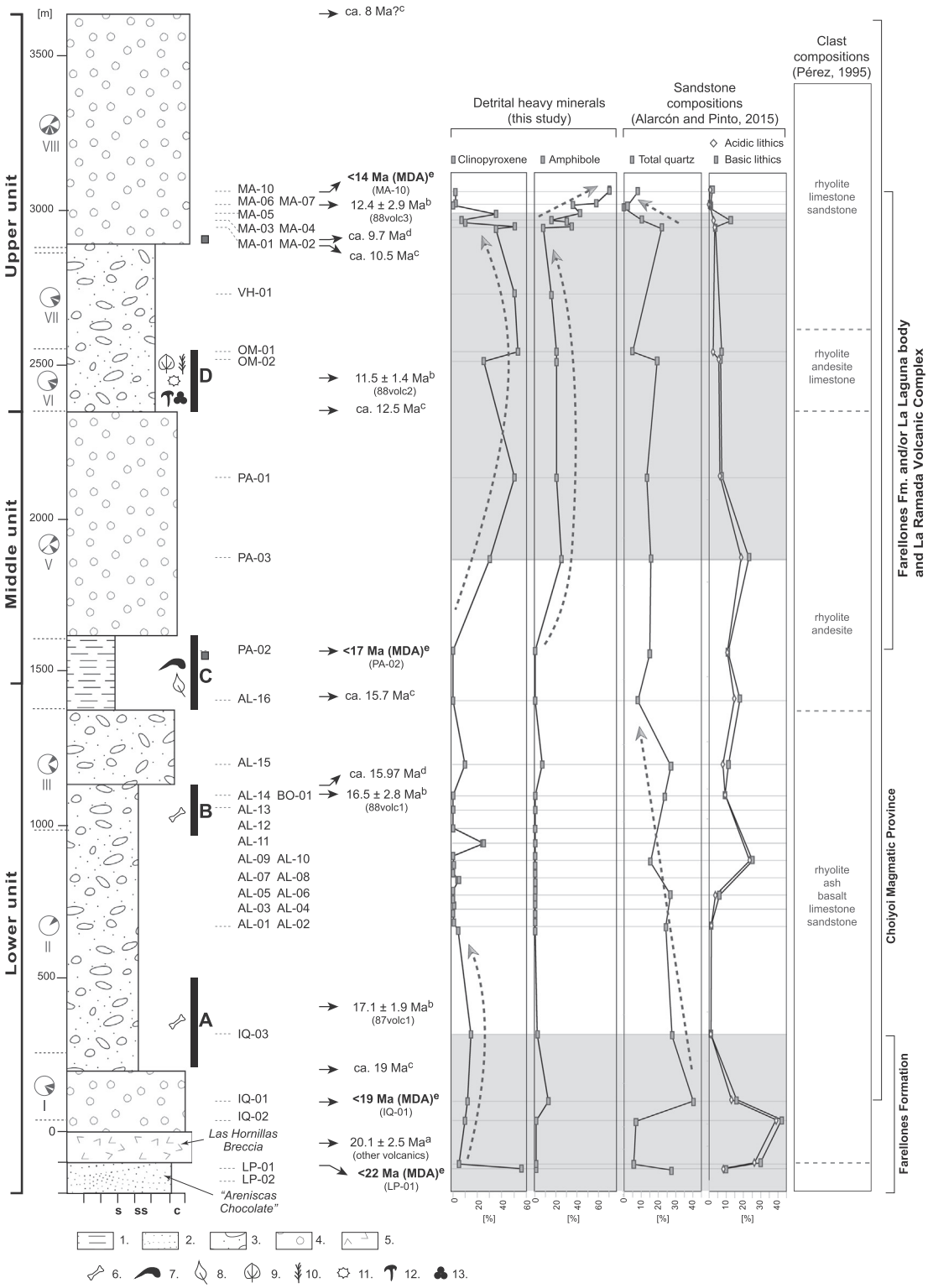

(caption on next page)

4. Samples and methodology

A variety of heavy mineral discrimination diagrams have helped to define specific characteristics and compositional trends of source rocks (e.g., Mange and Wright, 2007). For instance, analysis of major elements in amphibole, pyroxene, tourmaline and garnet (e.g., Krawinkel et al., 1999; von Eynatten and Gaupp, 1999; Sabeen et al., 2002; Pinto et al., 2004, 2007; Mange and Morton, 2007) can define specific metamorphic and igneous trends. Moreover, detrital zircon U–Pb dating has proved to be a powerful tool in studies of sedimentary provenance, crustal evolution, paleogeographic reconstructions and stratigraphic correlations (e.g., Mueller et al., 1994; Fedo et al., 2003; Cawood et al., 2007; Bahlburg et al., 2009). Also, detrital zircon age data are useful in providing depositional age limits for siliciclastic sedimentary successions (e.g., Levina et al., 2014; Brennan and Ridgway, 2015; Fosdick et al., 2015).

Fig. 5. Schematic column of the Chinches Formation based on the stratigraphy established by Jordan et al. (1996), showing the position of the analyzed samples, informal units of Chinches Formation, ages and percentages of detrital heavy minerals (clinopyroxenes, amphiboles), sandstone compositions (quartz, volcanic lithics) and clast compositions, from this and previous studies (Jordan et al., 1996; Pérez, 1995, 2001; Alarcón and Pinto, 2015). The clast compositions correspond to the Aldeco section elaborated by Pérez (1995); the approximate stratigraphic position of these data is based on correlations made by Jordan et al. (1996). The stratigraphic position in the region of the studied Chinches Formation is indicated in Fig. 3C; the lowest members after Mirré (1966) are indicated; the Conglomeratic Sandstones member corresponds to the succession between 0 and 3600 m as indicated. Geographical locations of samples are given in Fig. 6. *Ages*: 'a', age data given by Leveratto (1976) for a subvolcanic andesite at Barreal, and correlated by Pérez (2001) with the Las Hornillas breccia; 'b', age data given by fission tracks on zircons (Jordan et al., 1996); 'c', ages defined by magnetostratigraphy (Jordan et al., 1996); 'd', age defined by magnetostratigraphy (Ruskin et al., 2011); 'e': U–Pb maximum depositional ages (MDA) on detrital zircons (this study). See text for more details. *Symbols*: Grain-size: s, siltstone; ss, sandstone; c, conglomerate. *Lithologies*: 1. Limestones and sandstones, 2. Sandstones, 3. Conglomerates, sandstones, and siltstones, 4. Conglomerates, 5. Volcanic breccia. *Fossils*: 6. Vertebrates, 7. Bivalves, 8. Leaves, 9. Angiosperms, 10. Gymnosperms, 11. Spores, 12. Dinoflagellates, 13. Foraminifera. Black bars indicate approximate stratigraphic position of fossiliferous strata recognized in the Chinches Formation: A–B, fossil mammal assemblages (Marsupials, Xenarthra [Cingulata and Tardigrada], Notoungulates [four families], Litopterns and six groups of rodents) recognized along the Los Patos valley in the lower Chinches Formation, informally named "Chinches bearing level" (CBL) and "Las Hornillas bearing level" (LHBL) (López et al., 2011); these authors assigned the Santacrucian South American Land Mammal Ages (SALMA, ca. 18.5–16.3 Ma, Flynn and Swisher, 1995; Flynn et al., 2012; J.J. Flynn, personal communication) to these fossils; C, lacustrine deposits with leaves and bivalve shells (Jordan et al., 1996); D, tuffaceous deposits with herbaceous and shrubby elements with chlorococcaleans, scarce microforaminifera, and dinoflagellate cysts (Ottone et al., 1998, quoted in Pérez, 2001). Gray boxes next to the column indicate the location of stable isotopic values for carbonate units studied by Ruskin et al. (2011). On the left side of the column, qualitative paleocurrent data are presented accordingly to the eight facies groups defined by Jordan et al. (1996).

Sampling in the MFB was undertaken in the area between Las Hornillas in the east and the San Juan Refuge in the west, which contains the complete column of the sedimentary basin (Figs. 4, 5 and 6). Samples of sandstone and sandstone matrix from conglomerates were collected for heavy mineral analysis (n = 36), microprobe analysis (n = 14) and detrital zircon U–Pb geochronology (n = 4) (Fig. 5 and Table S1 in Supplementary Material). All three informal stratigraphic units (lower, middle and upper) of the Chinches Formation have been sampled in this study.

4.1. Heavy mineral analysis

Heavy mineral fractions (HM) were acquired from 36 samples (3–5 kg) following standard laboratory techniques described by Parfenoff et al. (1970) and Mange and Maurer (1992) at the Geology Department, Universidad de Chile. The 63–125 μm fraction was obtained by sieving. Heavy mineral separations were performed using a Gemeni table, a Franz Isodynamic Magnetic separator and bromoform (σ = 2.89 g/cm^3). We examined the 'light' minerals exiting the Gemeni to confirm the absence of heavy minerals. Approximately 400 grains per sample were point counted in order to determine the HM distribution. The results are presented in Table S1 (Supplementary Material). Of the 33 samples, 14 were selected for microprobe analysis. Around ten grains of each mineral per sample were taken when possible to be probed; a total of 211 grains (15 garnets, 87 amphiboles, 80 pyroxenes and 29 tourmalines) were analyzed using a Cameca SX50 electron microprobe fitted with three wavelength-dispersive spectrometers at the British Geological Survey, Keyworth, UK. Geochemical analyses of key detrital minerals are presented in Tables S2 and S3 (Supplementary Material). The procedure used an accelerating voltage

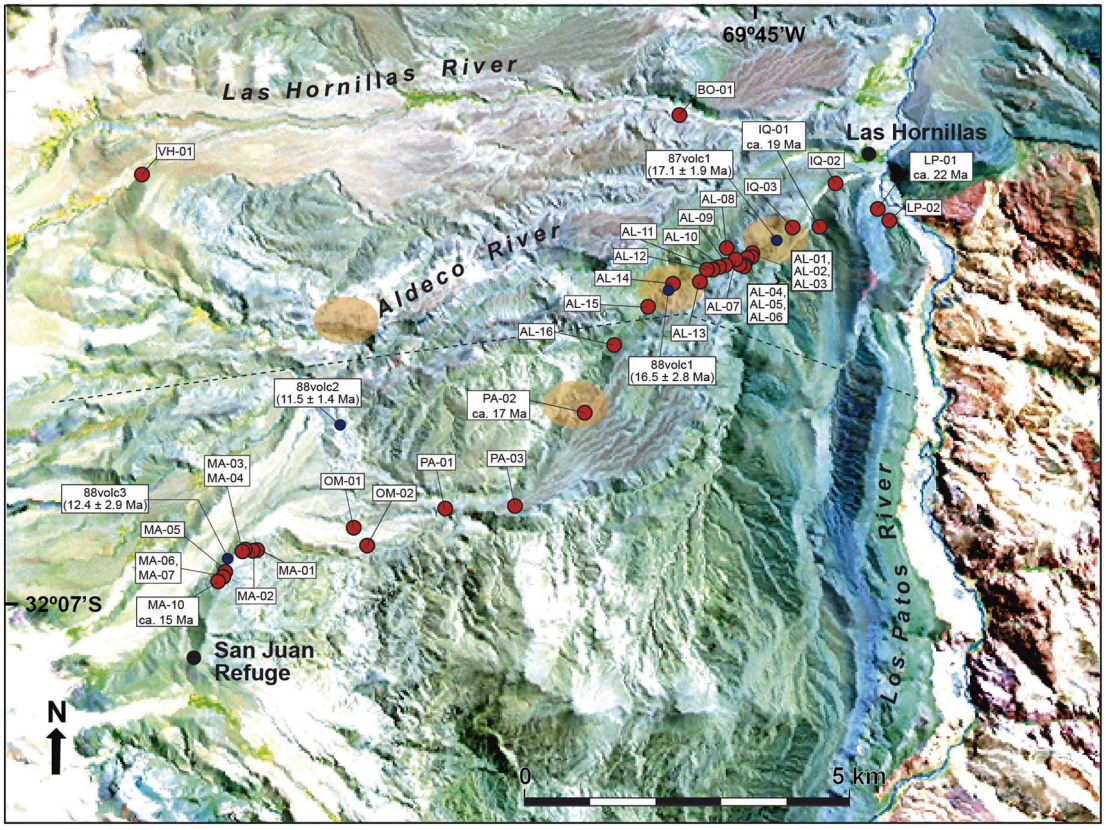

Fig. 6. LANDSAT–TM image with the location of the samples from this study (modified from Alarcón and Pinto, 2015) (red dots) and from Jordan et al. (1996) (blue dots). References of indicated ages as in Fig. 5. Approximate locations of fossiliferous strata reported by Jordan et al. (1996), Pérez (2001) and López et al. (2011) are indicated (orange ellipses). (For interpretation of the references to colour in this figure legend, the reader is referred to the web version of this article.)

of 15 kV, a sample current of 20 nA and a beam focused to approximately 1 μm. A mixture of natural minerals and synthetic materials were used for calibration, and raw data were processed using the Quantiview software provided by Cameca. Most of the tracer minerals could be identified easily given the researcher's experience. However, we analyzed 54 unknown mineral grains by X-ray diffraction, which proved to correspond mainly to epidote of several colors. The complete data set was used in classification and discrimination diagrams for interpretation of provenance (after Pinto et al., 2004, 2007; Rodríguez et al., 2012).

4.2. Detrital zircon U–Pb geochronology

Four medium grain-size sandstone samples from the Chinches Formation were prepared for U–Pb zircon geochronology: LP-01 and IQ-01 from the lower unit, PA-02 from the middle unit, and MA-10 from the upper unit (Fig. 5). Detrital zircons were concentrated from the heavy mineral fraction using a Frantz magnetic separation at 1.0 A. The resulting zircon separates were further concentrated by selectively removing other minerals under a binocular microscope at the Universidad de Chile.

One zircon sample (LP-01) was analyzed by U–Pb (LA–ICPMS) at the Laboratorio de Estudios Isotópicos (LEI), Geoscience Center, Universidad Nacional Autónoma de México (UNAM), Mexico. The other three samples (IQ-01, PA-02 and MA-10) were analyzed by U–Pb (LA–ICPMS) at Washington State University, USA. Sample coordinates, analytical methods, and U–Pb (LA–ICPMS) age measurements of zircon grains are available in Appendix S1 of Supplementary Material.

5. Results

5.1. Detrital heavy minerals

Clinopyroxene and amphibole are the most common heavy minerals in the Chinches Formation (Table S1, Supplementary Material), consistent with sourcing from a volcanic arc (Nechaev, 1991; Nechaev and Isphording, 1993). Amphiboles and clinopyroxenes are present in the lower part of the lower unit, the upper part of the middle unit, and throughout the upper unit of the Chinches Formation (Fig. 4); tourmalines, garnets, and zircons are present in subordinate amounts. The main characteristics of these minerals are given below.

5.1.1. Garnets

Garnets were recognized in two samples, PA-02 and MA-04, from the middle and upper units of the Chinches Formation, respectively (Table S1, Supplementary Material). Two series of garnets were defined, aluminous and calcic (Fig. 7A–B). The chemistry of the aluminous series can be analyzed using a diversity of discrimination diagrams to establish its provenance (e.g., Mange and Morton, 2007; Krippner et al., 2014; Stern and Wagreich, 2013). On the basis of discrimination diagrams (Fig. 7C), the aluminous garnets are likely to have a regional metamorphic source, mainly comprising metasedimentary rocks, probably of low-grade Barrovian-type metapelites with minor granulite facies metapelites (field 3 in Fig. 7C, after Morton et al., 2003). Other discrimination diagrams show a possible provenance from granites and granite pegmatites and biotite schists (field 1 in Fig. 7C, after Preston et al., 2002), or felsic and intermediate granulites and gneisses/amphibolites metamorphosed under amphibolite facies (fields 6 and 7 in Fig. 7C, after Méres, 2008). Four calcic garnet grains were recognized, one andradite and three grossulars (Fig. 7B). The most typical occurrence of such garnets is in contact or thermally metamorphosed calcareous sedimentary rocks and especially in associated metasomatic skarns (Deer et al., 1997).

5.1.2. Tourmalines

Tourmalines were mainly found in the middle Chinches Formation (Table S1, Supplementary Material), but are also present in some samples from the lower and upper units of this formation. They are generally scarce with a maximum content of 7%. Tourmalines analyzed from three samples correspond to alkali tourmalines (rich in Fe^{2+} and Mg^{2+}); most were classified as dravites (X_{Mg} = 0.56–0.77), with few grains classified as schorl (X_{Mg} = 0.25–0.45) (according to Henry et al., 2011). Tourmaline compositions are related to their paragenesis (e.g., Henry and Guidotti, 1985; Henry and Dutrow, 1996; Dutrow and Henry, 2000). On the Al–Mg–Fe diagram of Henry and Guidotti (1985) (Fig. 8A), they fall mainly in the field of metapelites and metapsammites coexisting with an Al-saturating phase. On the Ca–Mg–Fe plot (Fig. 8B), they fall in the field of Ca-poor metapelites, metapsammites and quartz–tourmaline rocks. Thus, considering both discrimination diagrams, detrital tourmalines from the middle Chinches Formation suggest derivation from metapelites and metapsammites.

5.1.3. Amphiboles

Amphiboles are present throughout the Chinches Formation, apart from the upper part of its lower unit and the base of its middle unit (Fig. 5, and Table S1 in Supplementary Material). All studied amphiboles have a well-preserved prismatic habit, typical of volcanic sources. Since amphiboles are known to be most abundant in rocks of intermediate composition, it is likely the amphiboles were mainly derived from intermediate volcanic rocks.

The studied amphiboles belong to the calcic group, with $^{B}(Mg,Fe^{2+},Mn^{2+},Li) \leq 0.50$, $^{B}(Ca,Na) \geq 1.00$ and $^{B}Na < 0.50$ apfu (atoms per formula unit) (Leake et al., 1997, 2004). Many of the amphiboles (43%, n = 38) are slightly titanian (0.25 < Ti < 0.49 apfu, see Table S2 in Supplementary Material). They are mainly pargasites and magnesio-hornblendes (Fig. 9A; after Hawthorne et al., 2012). In the lower unit (samples IQ-01 and IQ-03), all amphiboles have $(Na + K + 2Ca)_A \geq 0.5$ and correspond to pargasites. In the upper unit, pargasite is predominant, and amphiboles with $(Na + K + 2Ca)_A < 0.5$ corresponding to magnesio-hornblendes are subordinate. In samples MA-01, MA-02, and MA-05, magnesio-hornblende is absent (Fig. 9A). The samples from the top of the upper unit (MA-06, MA-07, and MA-10) contain significant quantities of magnesio-hornblende. It is worth noting that in these three samples, clinopyroxene is absent or very scarce (Table S1, Supplementary Material). Moreover, sample MA-06 contains exclusively magnesio-hornblende (Table S1, Supplementary Material), whereas the other two samples also have pargasite (Fig. 9A). The character of amphiboles from MA-06 suggests a local source rock contributed to this stratigraphic level, the influence of which progressively diminished upward in the sequence.

All amphiboles fall in the igneous domain on the Al^{VI} vs. Al^{IV} diagram (Fig. 9B) (after Leake, 1965), which is consistent with their volcanic habit. Moreover, some samples from the upper unit (MA-06, MA-07, and MA-10) are concentrated in a restricted domain of the diagram with low Al^{IV} contents, indicating specific igneous source rocks supplied them.

The Na + K vs. Al^{IV} diagram (Fig. 9C) is useful to discriminate between calc-alkaline amphiboles of island arc and continental arc origin (Jakes and White, 1972). Amphiboles from the upper Chinches Formation (MA-06, MA-07, and MA-10) fall in the calc-alkaline island arc domain, with the other samples falling in the calc-alkaline continental arc domain. In particular, many of the amphiboles from MA-02 and MA-05 fall in the Na + K and Al^{IV}-rich field defined by the amphiboles from the Farellones Formation, which was formed during a later phase of magmatic differentiation of the Oligo–Miocene arc (Rodríguez et al., 2012, and references therein).

In summary, detrital amphiboles from the Chinches Formation have a volcanic origin and fall into two main compositional groups. Those from the bottom of the lower unit (IQ-01 and IQ-03) and from the bottom of the upper unit (samples MA-02 to MA-05) mainly have pargasite compositions of volcanic origin with a calc-alkaline, acidic-intermediate and continental affinity. The second group, from the top of

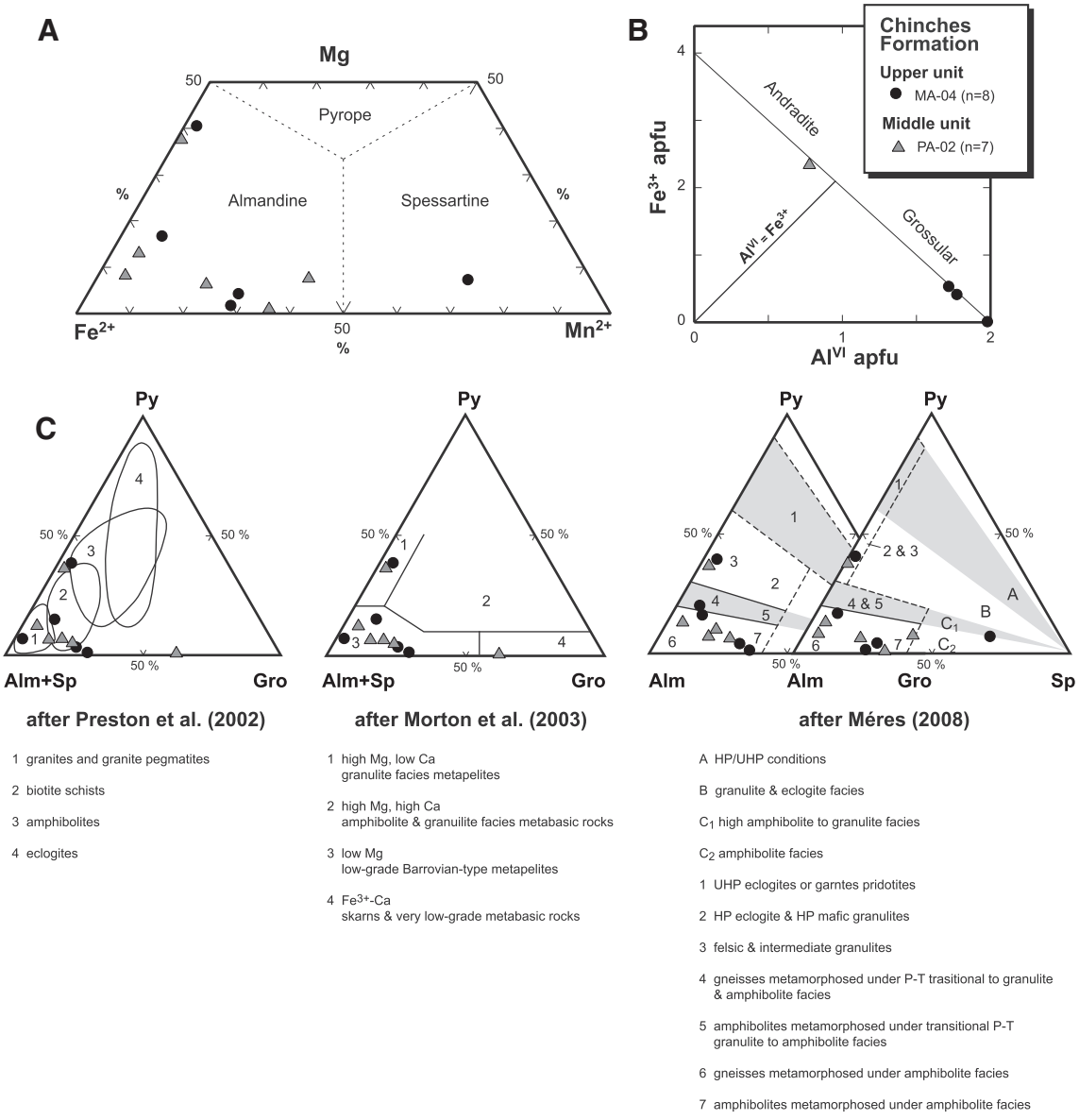

Fig. 7. (A) Compositional diagrams of detrital aluminous-series garnets (n = 15) from the Chinches Formation (after Deer et al., 1997); (B) Compositional diagram of detrital calcic garnets from the Chinches Formation (after Deer et al., 1997); (C) Aluminous-series garnet chemistry as a discriminator of sandstone provenance on diagrams proposed by Preston et al. (2002), Morton et al. (2003), Méres (2008) and Mange and Morton (2007), and modified from Stern and Wagreich (2013). Element concentrations are given in relative percentage on the ternary diagram and are based on their apfu (= atoms per formula unit).

the upper unit (MA-06, MA-07, and MA-10), mainly has magnesio-hornblende compositions of volcanic origin with a calc-alkaline, intermediate–basic and island arc affinity.

5.1.4. Clinopyroxenes

The detrital clinopyroxenes found in the Chinches Formation have augite and diopside compositions (Fig. 10A, and Table S3 in Supplementary Material) and are prismatic, typical of volcanic rocks. The diopsides have an alkaline affinity, whereas the augites are subalkaline (Fig. 10B) (Le Bas, 1962).

The content of Al in clinopyroxene is related inversely to the Si activity of magmas (Le Bas, 1962; Carmichael et al., 1970). Low SiO_2 activity suits the replacement of Si by Al^{IV} (Simonetti et al., 1996). Based on this character, Rodríguez et al. (2012) proposed that clinopyroxene with Al^{IV} apfu ≤ 0.050 is generated in acidic to intermediate rocks, and clinopyroxene with Al^{IV} apfu > 0.050 is generated in intermediate to basic rocks. On the basis of this criterium, most of the detrital clinopyroxenes from the Chinches Formation, have intermediate to basic character (n = 66), with only a few grains having acidic to intermediate character (n = 14) (Table S1 in Supplementary Material).

Leterrier et al. (1982) used Na, Ca, Al, Ti and Cr concentrations in clinopyroxene phenocrysts to discriminate the composition (alkaline, tholeiitic, and calc-alkaline) and geodynamic setting (orogenic, non-orogenic) for intermediate to basic rocks (Fig. 10C–E). The authors used the concept of 'orogenic' to refer types of rocks from convergent settings, and 'non-orogenic' to refer types of rocks from divergent settings. These diagrams can be used for detrital clinopyroxene of volcanic origin if the minerals are well preserved (Krawinkel et al., 1999; Pinto et al., 2004), which is the case for the Chinches Formation. The Ti vs. (Na + Ca) diagram shows that the majority of clinopyroxene have a subalkaline signature (n = 43), with a smaller number (n = 23) having an alkaline signature (Fig. 10C, and Table S1 in Supplementary Material). Within the subalkaline group, the clinopyroxene mainly falls in the orogenic domain (n = 29) (Fig. 10D, and Table S1 in Supplementary Material), consistent with the abundance of amphiboles of calc-alkaline

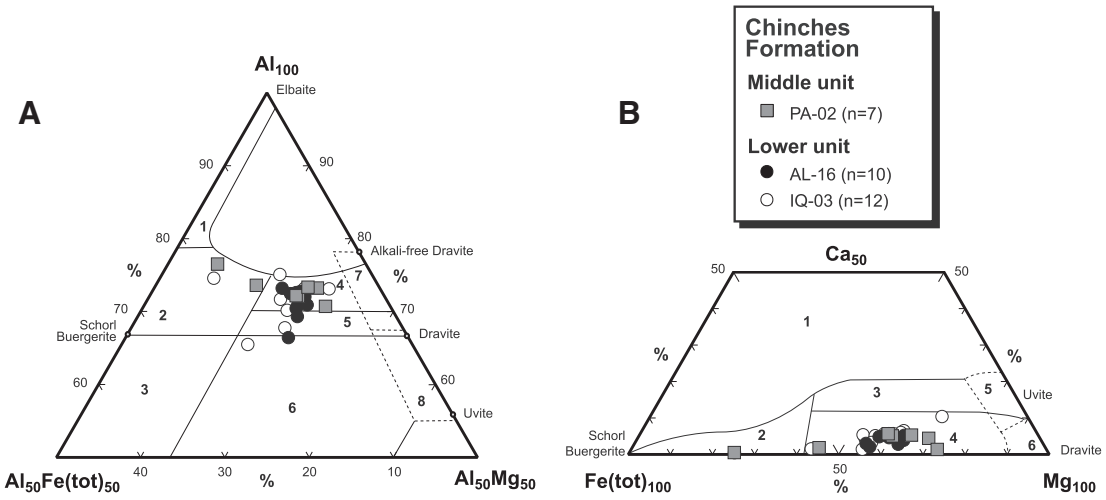

Fig. 8. Distribution of detrital tourmalines (n = 28) from the Chinches Formation on the discrimination diagram of Henry and Guidotti (1985). Element concentrations are given in relative percentage on the ternary diagram and are based on their apfu (= atoms per formula unit). (A) 1. Li-rich granitoid pegmatites and aplites; 2. Li-poor granitoids and their associated pegmatites and aplites; 3. Fe^{3+}-rich quartz–tourmaline rocks (hydrothermally altered granites); 4. Metapelites and metapsammites coexisting with an Al-saturating phase; 5. Metapelites and metapsammites not coexisting with an Al-saturating phase; 6. Fe^{3+}-rich quartz–tourmaline rocks, calcsilicate rocks, and metapelites; 7. Low-Ca meta-ultramafics and Cr, V-rich metasediments; and 8. metacarbonates and meta-pyroxenites. (B) 1. Li-rich granitoid pegmatites and aplites; 2. Li-poor granitoides and associated pegmatites and aplites; 3. Ca-rich metapelites, metapsammites, and calc-silicate rocks; 4. Ca-poor metapelites, metapsammites, and quartz-tourmaline rocks; 5. Metacarbonates, 6. Meta-ultramafics.

continental affinity for the same samples (Fig. 9C).

The clinopyroxenes from the bottom of the lower Chinches Formation have a subalkaline affinity, with only a few grains having alkaline character (Fig. 10C, Table S1 in Supplementary Material). Also in this unit, acidic clinopyroxene is rare. In particular, in sample IQ-01, intermediate–basic clinopyroxene grains have non-orogenic, orogenic and calc-alkaline affinities. The clinopyroxenes in sample AL-11, also from the lower Chinches Formation (Table S1, Supplementary Material), have mainly acidic character (Fig. 10C).

Clinopyroxene has not been analyzed from the middle Chinches Formation. In the upper Chinches Formation, acidic clinopyroxene is scarce, being absent in samples MA-04 and MA-05 (Table S1, Supplementary Material). Samples MA-02 and MA-05 contain mainly alkaline clinopyroxene, which is also present, but less commonly, in sample MA-04 (Fig. 10C). Several clinopyroxene grains in sample MA-03 fall in the non-orogenic domain (Fig. 10D and Table S1, Supplementary Material). Only samples MA-01, MA-03, and MA-05 from the upper Chinches Formation show a significant amount of clinopyroxene with intermediate–basic, orogenic and calc-alkaline character (Fig. 10C–E). Furthermore, clinopyroxene is absent in the samples from the top of the upper unit (MA-06, MA-07, and MA-10), correlated with a change in the associated amphibole compositions (Table S1, Supplementary Material).

In summary, clinopyroxenes in the Chinches Formation mainly have intermediate–basic compositions, predominantly with subalkaline affinities. An alkaline group is also present in the bottom of the upper Chinches Formation in samples where amphiboles have a calc-alkaline continental signature (mainly in samples MA-02 and MA-05, Table S1 in Supplementary Material). Most of the subalkaline clinopyroxenes have orogenic calc-alkaline affinities (Fig. 10E) and correlate positively with pargasite amphiboles and negatively with magnesio-hornblende amphiboles.

5.1.5. Evolution of heavy mineral provenance

The integration of amphibole and clinopyroxene data from detrital samples of the Chinches Formation indicates a clear progression of volcanic sources for the MFB. Amphiboles and clinopyroxenes can be grouped in four successive broad mineral associations (Fig. 5, Table S1 in Supplementary Material) and interpreted according to classic rock-forming mineralogical publications (e.g., Deer et al., 1962):

The first association, in the bottom of the lower unit (samples LP-02 to IQ-03), is characterized by supply from basic–intermediate rocks with orogenic calc-alkaline character, together with intermediate–acidic rocks with calc-alkaline non-orogenic continental character. This combination of data indicates two kinds of source rocks, possibly a calc-alkaline basaltic–andesitic rock and a calc-alkaline andesitic–dacitic rock.

The second association is found in the middle and upper part of the lower Chinches Formation and the basal part of the middle Chinches Formation (samples AL-01 to PA-02), where clinopyroxene and amphibole are almost absent, indicating a mainly non-volcanic or a very acidic volcanic source rock, such as rhyolites, which tend to lack these minerals.

The third association is rich in clinopyroxene and amphibole and occurs in the upper part of the middle Chinches Formation, and the lower part of the upper Chinches Formation (samples PA-03 to MA-05). There are two kinds of basic–intermediate clinopyroxene, one with alkaline compositions, and the other with orogenic calc-alkaline compositions. The associated amphiboles have calc-alkaline continental intermediate–acidic character. This association indicates three kinds of source rocks: alkaline basaltic andesite, calc-alkaline basalt–andesite, and calc-alkaline andesite–dacite.

The fourth association, from the top of the upper unit (samples MA-06 to MA-10), consists only of amphibole and was derived from calc-alkaline basaltic–andesitic rocks of island arc character.

These four associations describe clear changes in the source of the basin fill sandstones of the MFB (Fig. 5). The potential volcanic geological units that supplied the first subalkaline amphibole + clinopyroxene association to the lowest Chinches Formation (< 300 m, Fig. 5) probably belong to the Miocene Farellones Formation (Fig. 3) of continental affinity (Nyström et al., 2003). The second association in the lower and middle Chinches Formation (~700–1600 m, Fig. 5), where clinopyroxene + amphibole is almost absent, reflects a different source, probably corresponding to acidic Choiyoi Magmatic Province rocks (Fig. 5) (see below).

The sources contributing to the third and fourth associations are less clear. The third association in the middle and upper Chinches Formation (~1800–3000 m, Fig. 5) shows a mixing of alkaline and calc-alkaline signatures that probably indicates a variety of volcanic sources. The calc-alkaline continental source probably corresponds to the Miocene Farellones Formation (Fig. 3) of calc-alkaline continental character (e.g., Nyström et al., 2003). Alkaline and calc-alkaline island

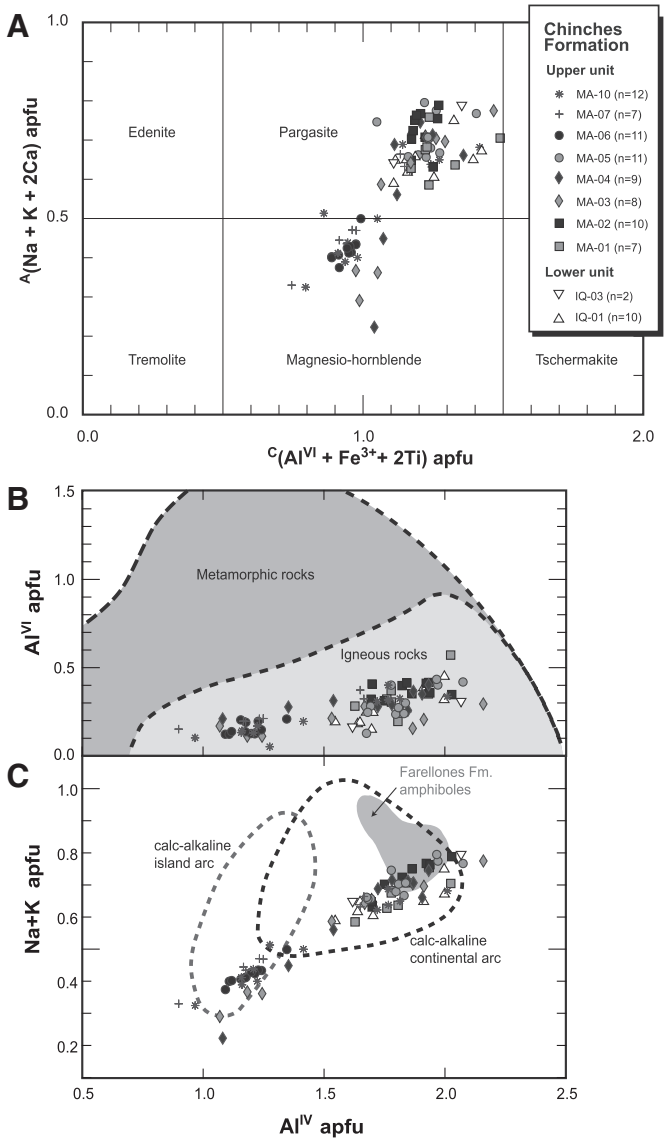

Fig. 9. Geochemistry of detrital amphiboles from the Chinches Formation: (A) Calcic amphiboles with $^{B}(Ca + \Sigma M^{2+})/\Sigma B \geq 0.75$ and $^{B}Ca/\Sigma B \geq {}^{B}\Sigma M^{2+}/\Sigma B$ (classification according to Hawthorne et al., 2012); (B) Amphiboles on Al^{VI} vs. Al^{IV} discrimination diagram of Leake (1965). Light gray: compositional field for amphiboles from igneous rocks. Dark gray: compositional field for amphiboles from metamorphic rocks. (C) Amphiboles on the alkalis versus Al^{IV} discrimination diagram (after Jakes and White, 1972). Compositional field of amphiboles in the Farellones Formation (33°–34°S) is shown (Data source: Rodríguez et al., 2012, and references therein). Element concentrations are given in apfu (= atoms per formula unit).

arc signatures have not been reported from volcanic rocks in the region (e.g., Pérez, 1995; Pérez and Ramos, 1996; Rivano et al., 1993). We propose the La Ramada Volcanic Complex as a potential source of the geochemical signatures in the third and fourth associations in the middle and upper Chinches Formation (> 1800 m, Fig. 5), since this volcanic complex has been interpreted as representative of back-arc volcanism (Pérez and Ramos, 1996).

The absence of orthopyroxene throughout the succession is remarkable, since this mineral is a common component of heavy mineral assemblages derived from volcanic arcs (Nechaev, 1991). The lack of orthopyroxene provides further support for derivation from the Farellones Formation, since these volcanics are known to be orthopyroxene-poor at the latitudes of the MFB (Jara, 2013).

Finally, the scarce aluminous garnets and tourmalines are likely to be derived from metapelites and/or metapsammites. Since regional metamorphic rocks have not been reported in the region, we propose that these garnets and tourmalines represent material recycled from Mesozoic rocks of the Principal Cordillera (see discussion below). The similarly scarce calcic garnets could come from thermally metamorphosed calcareous sedimentary rocks from the Mesozoic succession.

5.2. Detrital zircon U–Pb ages

For sample LP-01 (Basal lower Chinches Formation: Areniscas Chocolate member, Fig. 5), a total of 95 zircon grains were dated by U–Pb LA–ICPMS method, but 18 were excluded due to high discordance and/or uncertainty (Fig. 11A, Table 1, and Table S4 in Supplementary Material). Reliable ages range between 20.9 ± 0.4 Ma and 1398 ± 35 Ma. The main group of ages ranges between ca. 20.9 and 57 Ma (~52%; Paleocene–early Miocene) with a maximum peak at ca. 22 Ma and a second peak at ca. 35 Ma. There are three smaller groups, one with an early Permian–Early Triassic age (~10%; ca. 250–277 Ma) with a peak at ca. 262 Ma, one with a Mesoproterozoic age (~9%) with a peak at ca. 1160 Ma, and one with Neoproterozoic to early Paleozoic ages (~13%; ca. 415–935 Ma). The detrital zircon grains also include Cretaceous (n = 4; ca. 68–97 Ma), Jurassic (n = 1; ca. 187 Ma), Late Triassic (n = 4; ca. 222–229 Ma), and early Carboniferous (n = 2; ca. 327–344 Ma) ages.

For sample IQ-01 (Lower unit Chinches Formation: basal Conglomeratic Sandstone member, Fig. 5), one hundred and fifteen zircon grains were analyzed by U–Pb LA–ICPMS method, with two rejected due to high discordance and/or uncertainty (Fig. 11B, Table 1, and Table S4 in Supplementary Material). The 113 best ages range from 17.5 ± 0.5 Ma to 2247.7 ± 17.1 Ma. The main population comprises ages between ca. 238 and 296 Ma (~71%; early Permian–Late Triassic) with a strong peak at ca. 256 Ma. A second population shows ages between ca. 17.5 and 42.3 Ma (~10%; Eocene–early Miocene) with peaks at ca. 19, ca. 22 and ca. 41 Ma. Also, there are zircons with Cretaceous (n = 3; ca. 66–92 Ma), Late Triassic (n = 6; ca. 220–236 Ma), Carboniferous (n = 2; ca. 305–328 Ma), Neoproterozoic to early Paleozoic (n = 5; ca. 363–921 Ma), and Mesoproterozoic (n = 5; ca. 1019–1351 Ma) ages. A single Paleoproterozoic zircon (ca. 2248 Ma) is also present.

For sample PA-02 (Basal middle Chinches Formation: middle Conglomeratic Sandstone member, Fig. 5), a total of 119 zircon grains were dated by U–Pb LA–ICPMS method in this sample (Fig. 11C, Table 1, and Table S4 in Supplementary Material). No data were excluded and ages range between 16.9 ± 0.7 Ma and 2941.6 ± 48.6 Ma. The probability density plot shows a multimodal distribution with several main peaks. The main group of ages is early Permian–Late Triassic (~45%; ca. 240–296 Ma) with two peaks at ca. 252 and ca. 270 Ma. Subordinate populations are represented by Neoproterozoic to early Paleozoic zircon ages (~16%; ca. 371–973 Ma; peaks at ca. 390, ca. 530, and ca. 623 Ma) and late Mesoproterozoic zircons (~16%; ca. 1026–1377 Ma; main peak at ca. 1106 Ma). Minor groups are ca. 16.9–63.8 Ma (~9%; Paleocene–Miocene; peaks at ca. 17 and ca. 49 Ma), ca. 68–161 Ma (~9%; Jurassic–Cretaceous; peak at ca. 154 Ma), and ca. 307–333 Ma (~5%; Carboniferous). A single Mesoarchean zircon (ca. 2942 Ma) is also present.

For sample MA-10 (Top upper Chinches Formation: upper Conglomeratic Sandstone member, Fig. 5), 117 zircon grains were analyzed by U–Pb LA–ICPMS method, with two being excluded (Fig. 11D, Table 1, and Table S4 in Supplementary Material). The 115 best ages lie between 13.3 ± 0.5 Ma and 1874.8 ± 25.4 Ma, with two main peaks. The largest is at ca. 250 Ma, which comprises ages between ca. 240 and 288 Ma (~59%; early Permian–Late Triassic), and the other is at ca. 15 Ma with ages between ca. 13.3 and 49.9 Ma (~17%; Eocene–Miocene). There are minor groups in the late Mesoproterozoic (~7%; ca. 1039–1336 Ma), Neoproterozoic to early Paleozoic (~6%; ca. 365–700 Ma), and Jurassic (~4%; ca. 151–186 Ma). The range of detrital zircons also includes Cretaceous (n = 2; ca. 102–128 Ma), Late

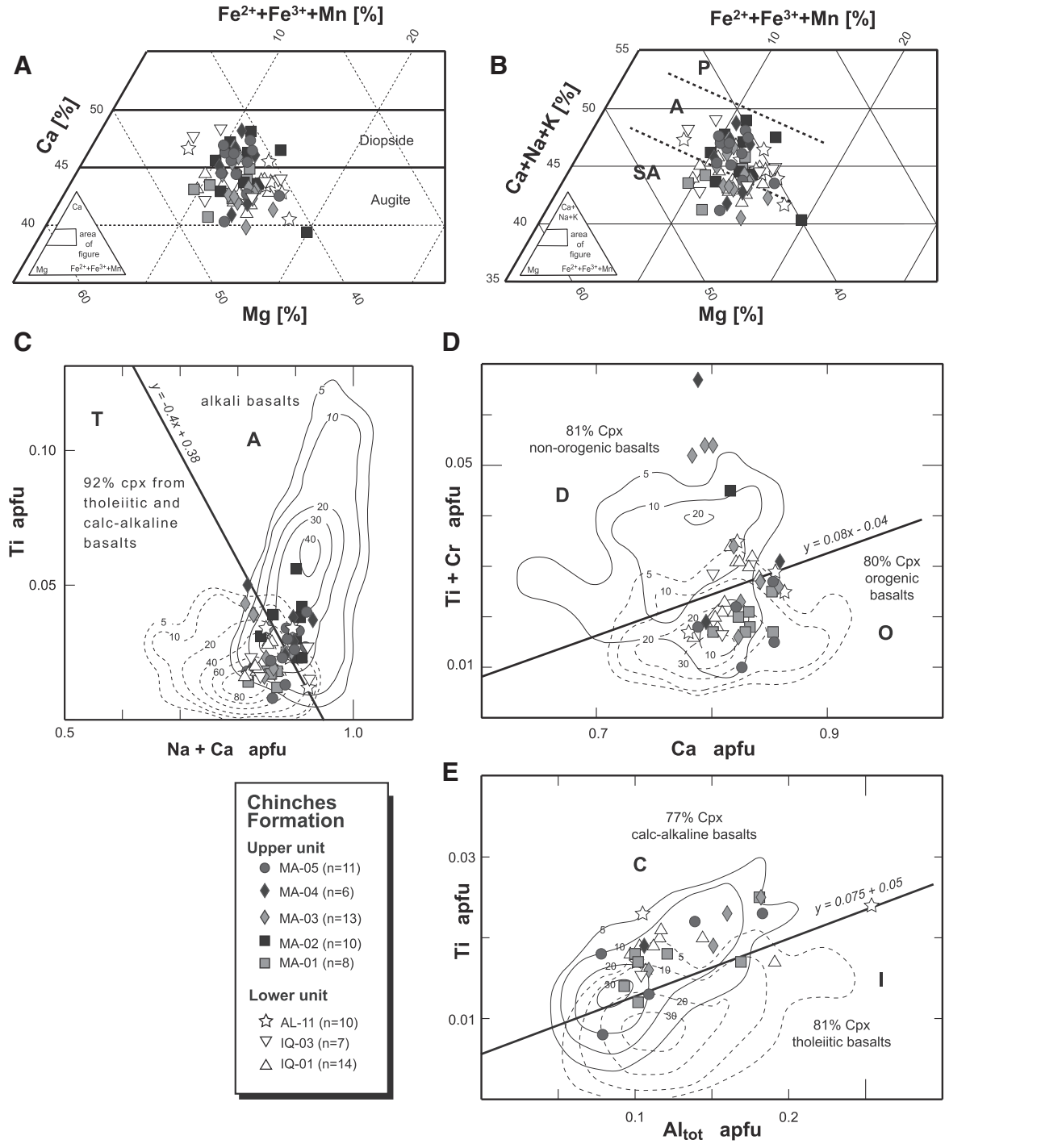

Fig. 10. Geochemistry of detrital clinopyroxenes: (A) Classification graphic of clinopyroxene proposed by Morimoto (1988); (B) Discrimination diagram proposed by Le Bas (1962), which indicates the alkali character of clinopyroxene (SA, subalkaline; A, alkaline; P, peralkaline); (C–D–E) Discrimination diagrams for basic clinopyroxenes proposed by Leterrier et al. (1982). *Domains*: T: tholeiitic and calc-alkaline, A: alkaline, D: non-orogenic, O: orogenic; C: calc-alkaline, and I: tholeiitic. Element concentrations are given in apfu (= atoms per formula unit).

Triassic (n = 3; ca. 230–237 Ma), Carboniferous (n = 2; ca. 301 Ma), and Paleoproterozoic (n = 1; ca. 1875 Ma) ages.

6. Discussion

6.1. Age of the Manantiales Foreland Basin

The youngest zircon U–Pb ages of detrital zircons are commonly used to constrain the maximum depositional age of siliciclastic sedimentary successions (Fedo et al., 2003; Gehrels, 2014). Therefore, the maximum depositional age of samples from Chinches Formation was evaluated on the basis of the detrital zircon U–Pb ages presented herein by using the age given by the mean age of the youngest cluster of grains (Table 2 and Fig. 11; age measurements in Table S4 in Supplementary Material).

The youngest age group calculated from zircon grains of sample LP-01 is 22.0 ± 0.4 Ma (n = 20; error of 95% conf.; MSWD = 2.2), and of sample IQ-01 is 18.6 ± 2.0 Ma (n = 3; error of 95% conf.; MSWD = 2.0) (Table 2 and Fig. 11A–B). These ages indicate an early Miocene (ca. 22–19 Ma) maximum depositional age for the lower

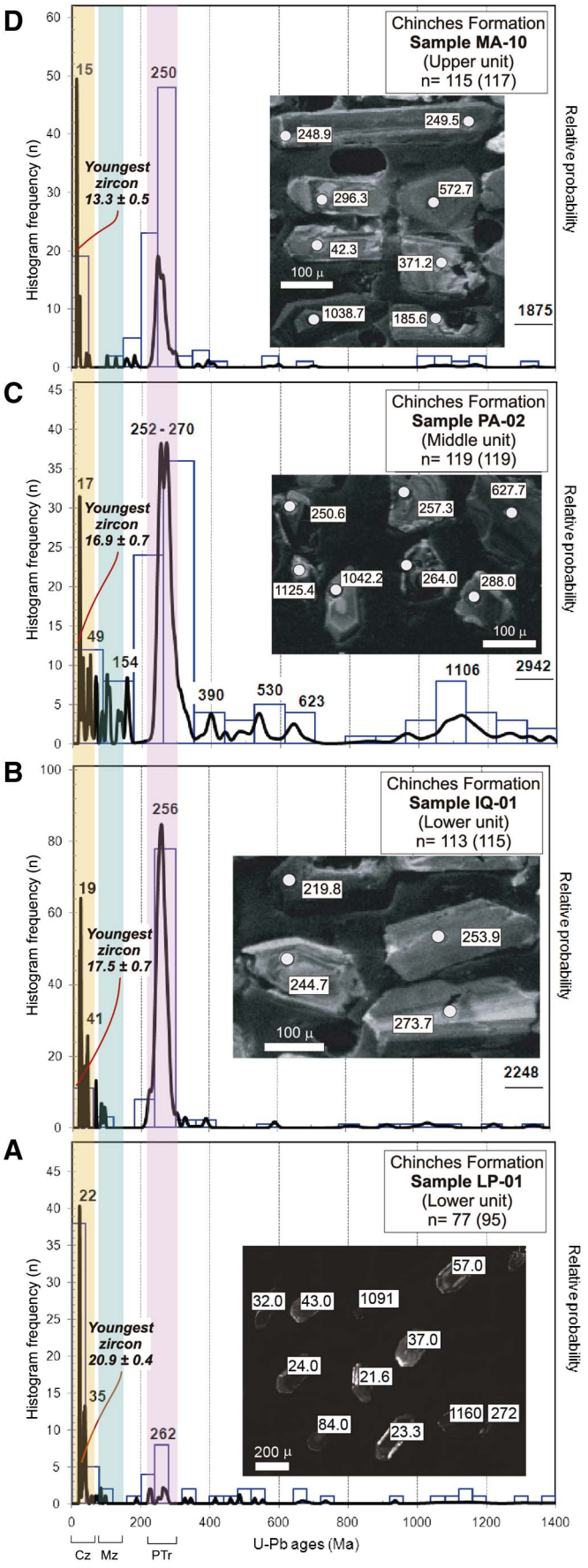

Fig. 11. Frequency histograms and relative probability plots of U–Pb ages on detrital zircons from the Chinches Formation of the samples: (A) LP-01, (B) IQ-01, (C) PA-02, (D) MA-10. Insets are cathodoluminescence images of the zircon grains from the study samples; spots are also showed with their ages (Ma). The three age populations related to the identified main sources are highlighted: PTr (Permo–Triassic Choiyoi Magmatic Province), Mz (Mesozoic sedimentary rocks), and Cz (Cenozoic igneous rocks).

Chinches Formation. The youngest detrital zircon group in sample PA-02 indicates an age of 17.1 ± 1.0 Ma (n = 2; MSWD = 0.1; Table 2 and Fig. 11C), early Miocene, as the maximum depositional age for the middle Chinches Formation. The youngest age group calculated from zircon grains of sample MA-10 is 14.5 ± 0.4 Ma (n = 13; error of 95% conf.; MSWD = 2.0; Table 2 and Fig. 11D), middle Miocene, as the maximum depositional age for the upper Chinches Formation. The maximum depositional ages define a coherent temporal trend through the succession, from < 22 Ma (LP-01) and < 19 Ma (IQ-01) at the base, to < 17 Ma (PA-02) in the middle and < 15 Ma (MA-10) at the top (Table 2 and Fig. 11). Next, we analyze these ages using previous chronological data in the study area (Fig. 12).

The maximum age of deposition, ca. 22 Ma, of the Areniscas Chocolate member in the lower Chinches Formation (Mirré, 1966) (Fig. 5), is the first geochronological assignation for this part of the succession. This age is in agreement with the estimated age for the Las Hornillas breccia member, ca. 20 Ma (Pérez, 2001), which overlies sample LP-01 (Fig. 12). The dated sample (LP-01) was taken from the green sandstones in the upper Areniscas Chocolate member (after Mirré, 1966) (Fig. 5, and Table S1 in Supplementary Material). Therefore, additional ages are needed to constrain the age of the older part of the member.

The maximum depositional age obtained from sample IQ-01, ca. 19 Ma (lower Chinches Formation, Fig. 5), is in agreement with the estimated age for the Las Hornillas breccia member (ca. 20 Ma), which just underlies sample IQ-01 (Fig. 12). The age also agrees with the zircon fission track age of 17.1 ± 1.9 Ma from a volcanic ash horizon (Jordan et al., 1996) from a sample stratigraphically above sample IQ-01 (Figs. 5 and 12). The maximum depositional age of ca. 17 Ma, in the middle Chinches Formation (PA-02), is slightly older than the previous reported ages for nearby strata (Fig. 12). Ruskin et al. (2011) re-correlated the magnetic polarities from Jordan et al. (1996) with Ogg and Smith (2004) and thus re-assigned a magnetostratigraphy age of ca. 15.7 Ma to the lacustrine deposits at ~1500 m, near sample PA-02 (Figs. 5 and 12). Moreover, fossil mammal assemblages from this part of the succession (Figs. 5 and 12, López et al., 2011) have been assigned to the Santacrucian South American Land Mammal Ages (SALMA, latest early Miocene, ca. 18.5–16.3 Ma) (Flynn and Swisher, 1995; Flynn et al., 2012; J.J. Flynn, personal communication). Furthermore, an age of ca. 16.8 ± 0.2 Ma (U–Pb, zircons) has been reported for a lapilli tuff within the lower Chinches Formation in the southern Los Caballos River (Mazzitelli et al., 2015). These geochronological, magnetostratigraphic and paleontological data constrain the age of the lower Chinches Formation (from IQ-01 to PA-02) as early Miocene, ca. 19–16 Ma (Fig. 12).

Finally, the maximum depositional age of ca. 15 Ma obtained from detrital zircons in sample MA-10 of the upper Chinches Formation (~3100 m, Figs. 5 and 11) is in agreement with previous geochronological and magnetostratigraphic data (Fig. 12). Jordan et al. (1996) gave two zircon fission-track ages (11.5 ± 1.4 Ma and 12.4 ± 2.9 Ma) for tuffaceous deposits in the upper Chinches Formation at ~2500 m and ~3000 m respectively (Figs. 5 and 12). Based on these geochronological data and complemented with magnetostratigraphy, Jordan et al. (1996) and Ruskin et al. (2011) proposed ages of ca. 10.5 Ma for the base of the upper Chinches Formation (~2800 m) and ca. 9.7 Ma for the base of the upper conglomerates in the succession (~3000 m) (Figs. 5 and 12). Therefore, the maximum depositional age of ca. 15 Ma obtained for sample MA-10 appears to be older than the true depositional age (Fig. 12).

Table 1
Percentage of representative U–Pb age groups in the four sedimentary rocks from the Chinches Formation.

Age range visible in samples	LP-01	IQ-01	PA-02	MA-10
	[%]	[%]	[%]	[%]
Oligo–Miocene (9–34 Ma)	32 (n = 25)	7 (n = 8)	5 (n = 6)	15 (n = 17)
Eocene (34–56 Ma)	19 (n = 15)	3 (n = 3)	3 (n = 3)	2 (n = 2)
Paleocene (56–66 Ma)	1 (n = 1)	–	1 (n = 1)	–
Cretaceous (66–145 Ma)	5 (n = 4)	3 (n = 3)	6 (n = 7)	2 (n = 2)
Jurassic (145–201 Ma)	1 (n = 1)	–	3 (n = 3)	4 (n = 5)
Late Triassic (201–237 Ma)	5 (n = 4)	5 (n = 6)	–	3 (n = 3)
Early Permian–Late Triassic (237–298 Ma)	10 (n = 8)	71 (n = 80)	45 (n = 54)	59 (n = 68)
Carboniferous (298–359 Ma)	3 (n = 2)	2 (n = 2)	5 (n = 6)	2 (n = 2)
Neoproterozoic–early Paleozoic (359–1000 Ma)	13 (n = 10)	4 (n = 5)	16 (n = 19)	6 (n = 7)
Mesoproterozoic (1.0–1.6 Ga)	9 (n = 7)	4 (n = 5)	16 (n = 19)	7 (n = 8)
Paleoproterozoic (1.6–2.5 Ga)	–	1 (n = 1)	–	1 (n = 1)
Archean (> 2.5 Ga)	–	–	1 (n = 1)	–

Table 2
Main U–Pb age pattern of dated Chinches Formation samples. Samples are in stratigraphic order.

Sample		Age (Ma)	n	MSWD*	error estim.
MA-10	oldest age	1875 ± 4	1	–	1 sigma
n_t = 115	youngest age	13.3 ± 0.5	1	–	1 sigma
uCh	youngest main group	14.5 ± 0.4	13	2.0	95% conf.
PA-02	oldest age	2942 ± 49	1	–	1 sigma
n_t = 119	youngest age	16.9 ± 0.7	1	–	1 sigma
mCh	youngest main group	17.1 ± 1.0	2	0.1	95% conf.
IQ-01	oldest age	2290 ± 109	1	–	1 sigma
n_t = 113	youngest age	17.5 ± 0.7	1	–	1 sigma
lCh	youngest main group	18.6 ± 2.0	3	2.0	95% conf.
LP-01	oldest age	1400 ± 9	1	–	1 sigma
n_t = 77	youngest age	20.9 ± 0.4	1	–	1 sigma
lCh	youngest main group	22.0 ± 0.4	20	2.2	95% conf.

lCh: lower Chinches Formation; mCh: middle Chinches Formation; uCh: upper Chinches Formation. *MSWD: mean square weighted deviation; n: number of zircon grains considered.

6.2. Provenance

Cenozoic sources for detrital zircons are dominant in the lowest member of the Chinches Formation (LP-01, Table 1 and Fig. 11). The oldest Cenozoic zircon peaks (ca. 35 Ma in LP-01, ca. 41 Ma in IQ-01, and ca. 49 Ma in PA-02) in the Chinches Formation indicate Eocene source rocks. Eocene igneous rocks can be found in the Paleogene plutonic belt (Parada et al., 2007), which crops out westward along the Principal Cordillera of Chile (e.g., ca. 55–47 Ma, Fredes Unit, Rivano et al., 1993). Zircons with late Oligocene to Middle Miocene ages (peaks at ca. 22 Ma in LP-01, ca. 19 Ma in IQ-01, ca. 17 Ma in PA-02, and ca. 15 in MA-10) are likely to have been derived from the Andean magmatic arc, which form large exposures of volcanic rocks, located to the west of the basin along the Chilean–Argentinean border (e.g., Abanico and Farellones Formations, Laguna del Pelado Volcanic Complex, La Laguna subvolcanic body, Fig. 3) (Rivano et al., 1990, 1993; Cristallini and Cangini, 1993; Pérez and Ramos, 1996; Mpodozis et al., 2009; Jara and Charrier, 2014).

Detrital zircons of Jurassic–Cretaceous age are almost absent in samples LP-01 and IQ-01 at the base of the lower Chinches Formation (Table 1 and Fig. 11). Jurassic–Cretaceous sources are best represented in the middle Chinches Formation (PA-02), with ~9% of the total population (peak at ca. 154 Ma) and the upper Chinches Formation (MA-10) with ~6% of the population (ca. 102–186 Ma). The scarcity of Jurassic–Cretaceous zircons in the succession is unexpected, considering that several works have identified Mesozoic sedimentary and volcanic clasts in conglomerates of the Chinches Formation (Iglesia Llanos, 1995; Jordan et al., 1996; Pérez, 2001). The small number of zircon grains with these ages is probably related to the overall more basic, and therefore zircon-poor, character of the Mesozoic igneous rocks (Tordillo Formation, Álvarez et al., 1995; Río Damas Formation, Aguirre et al., 2009).

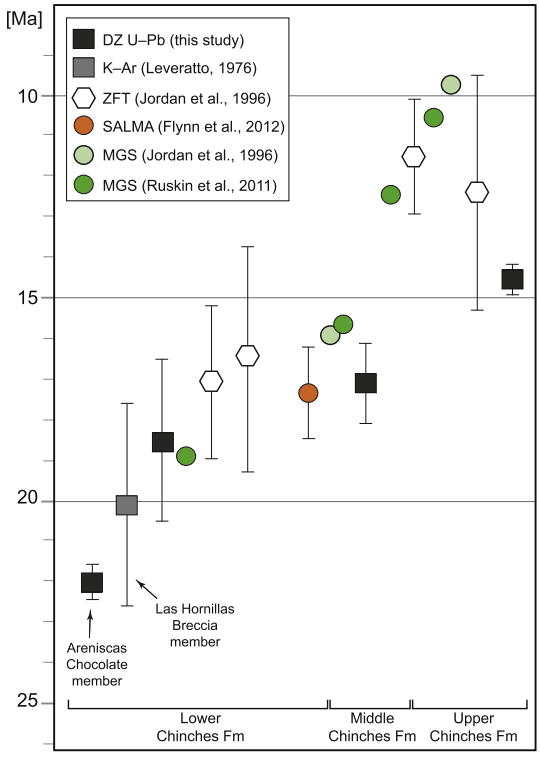

Fig. 12. Correlation of youngest detrital zircon ages from Chinches Formation with previous chronological data in the study area. Data are in stratigraphical order from left to right, and are based on data from Fig. 5. *Abbreviations*: DZ U–Pb, Detrital Zircon U–Pb ages; ZFT, Zircon Fission Track ages; SALMA, Santacrucian South American Land Mammal Ages; MGS, Magnetostratigraphic ages. See text for more details.

Early Permian-Late Triassic source rocks become dominant and Cenozoic source rocks subordinate in the sample above the Las Hornillas breccia member (Table 1 and Fig. 11). Early Permian–Late Triassic zircons form ~71% of the population in IQ-01 (peak at ca. 256 Ma), ~45% in PA-02 (peaks at ca. 252 and ca. 270 Ma) and ~59% in MA-10 (peak at ca. 250 Ma, Table 1). The change in provenance is also indicated by the decrease up-section of volcanic heavy mineral tracers (amphibole and clinopyroxene) from sample IQ-01 (Fig. 5 and Table S1, Supplementary Material). Therefore, above the Las Hornillas breccia member, the detrital zircon evidence indicates that the Choiyoi Magmatic Province became the dominant source of material to the MFB. Choiyoi magmatic rocks are widely exposed in the western

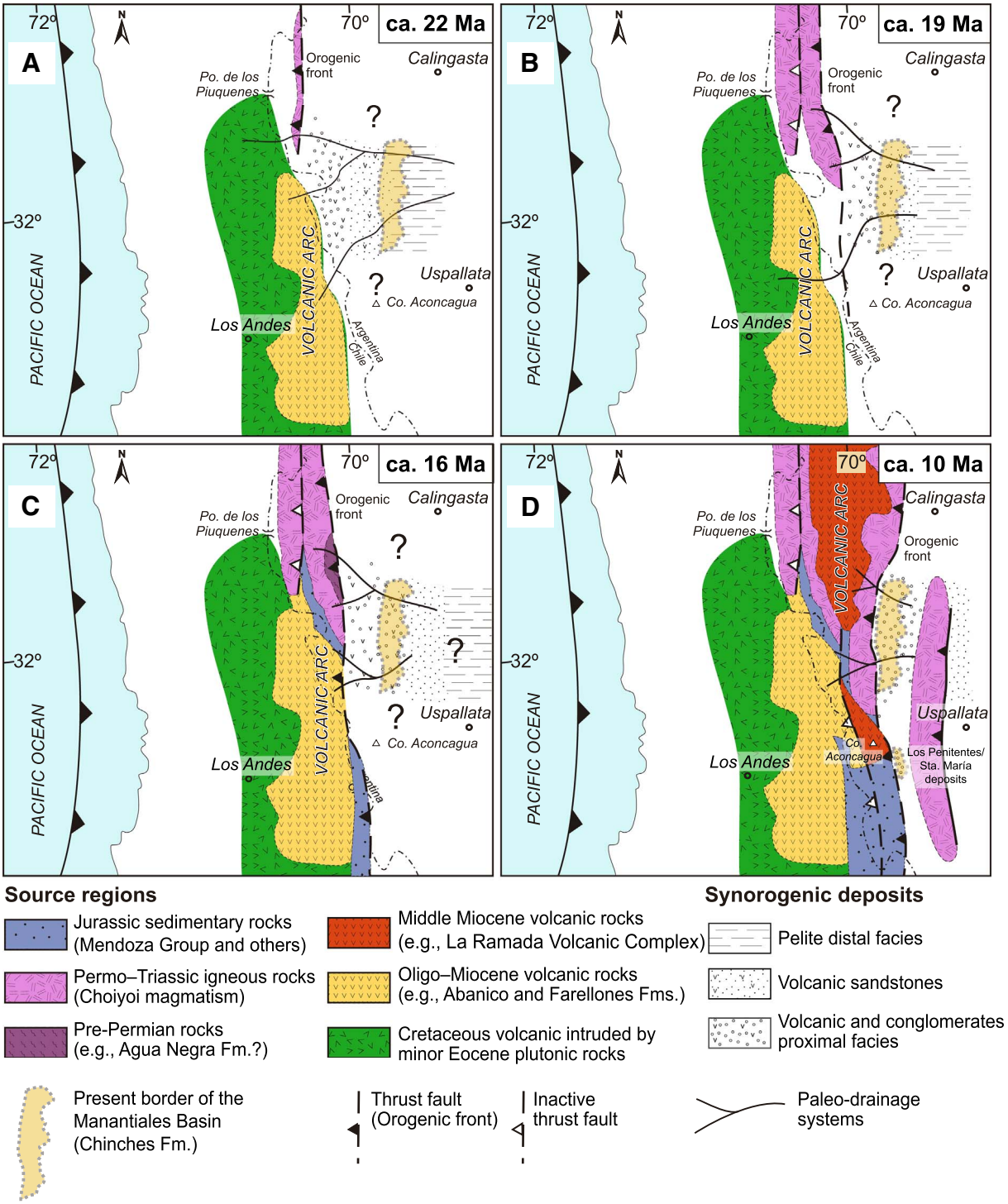

Fig. 13. Provenance evolution of the MFB based on the results of this study and previous published data (Iglesia Llanos, 1995; Jordan et al., 1996; Pérez, 1995, 2001; Ruskin et al., 2011; López et al., 2011; Alarcón and Pinto, 2015): (A) ca. 22 Ma; (B) ca. 19 Ma; (C) ca. 16 Ma; (D) ca. 10 Ma.

Frontal Cordillera to the west of the basin (Fig. 3), and are dated as ca. 286–247 Ma (Sato et al., 2015). The presence of a minor peak at ca. 262 Ma in the lowermost sample (LP-01, Figs. 5 and 11A) suggests that Choiyoi igneous rocks were already exposed during the earliest stages of sedimentation in the MFB, at least as a low paleorelief in the proto-Frontal Cordillera.

The sample from the middle Chinches Formation (PA-02) has a distinctively different zircon provenance compared with the other samples, showing abundant pre-Permian ages (Mesoarchean to Devonian) (Table 1 and Fig. 11). Mesoproterozoic (~16%) and Neoproterozoic–early Paleozoic (~16%) zircons are significant in sample PA-02, but form only trace amounts in the other samples. In addition, there are three grains of Mesoarchean to Paleoproterozoic age (2942 Ma in PA-02, 2248 in IQ-01, and 1875 Ma in MA-10 Ma). Basement rocks with these ages are not known in the vicinity of the MFB, but are represented in the basement of the Precordillera and Pampean Ranges to the east of the MFB (Rapela et al., 2010; Naipauer et al., 2010; Varela et al., 2011; and references therein). However, derivation from these ranges to the east is inconsistent with the paleocurrents, which indicate a main supply from the west (Fig. 5) (Jordan et al.,

1996). Although Mesoproterozoic–Devonian ages have been recorded in the Coastal Cordillera of Chile to the west (Álvarez et al., 2011) and in the Frontal Cordillera ~150 km to the south (Ramos and Basei, 1997), these outcrops are located too far from the MFB to be a source of detritus. In the case of Coastal Cordillera, it can not be a source because the western Principal Cordillera defined the water divide since the beginning of the MFB (Cristallini and Ramos, 2000). Mesoproterozoic–Devonian rocks in the southern Frontal Cordillera are not a possible source considering that the paleocurrents indicate sources from the west and east and not from the south (Jordan et al., 1996).

6.3. Recycling of Mesoproterozoic–Devonian zircons

Mesoproterozoic to Devonian detrital zircons equivalent to those found in the MFB have also been found in strata from the Miocene Cacheuta Foreland Basin (~33°S, Mendoza, Figs. 1C and 2A) (Buelow et al., 2014) and the Alto Tunuyán Foreland Basin (33°40′S) (Giambiagi et al., 2003; Porras et al., 2016) to the southeast and south respectively. For the Alto Tunuyán Basin, Porras et al. (2016) interpreted these ages as recycled from Mesozoic rocks of the Principal Cordillera, and this explanation could be the case for the Pre-Permian detrital zircons in the MFB. The strong correlation between abundance of Devonian and Mesoproterozoic zircon ages in the Chinches Formation suggests that all of these zircons probably come from the same source, such as the Mesozoic rocks in the Principal Cordillera at the studied latitudes (Fig. 3). Moreover, the presence of zircons of these ages throughout the Chinches Formation is consistent with the conglomerate clast count (Pérez, 2001), which indicates continuous supply from Mesozoic rocks. Oliveros et al. (2012) found Mesoproterozoic detrital zircons (ca. 1070 and ca. 1090 Ma) in the Upper Jurassic Lagunillas Formation (= Tordillo and Río Damas Formations, ca. 150 Ma) in the northern Chilean Andes (~28°S), together with Ordovician, Permian and Jurassic zircons, supporting this idea. Moreover, the almandine–pyrope garnets of metamorphic origin found in sample PA-02 are probably derived from recycled material.

6.4. Analysis of the paleogeographic evolution of the Manantiales Foreland Basin

In this section, we discuss the significance of detrital heavy minerals and detrital zircon U–Pb ages in terms of the evolution model of the MFB and tectonic events in the Principal and Frontal Cordilleras. We base our analysis on the stratigraphy defined by Jordan et al. (1996), using the heavy mineral and geochronological data from this study and compositional data of conglomerates and sandstones given by Mirré (1966), Pérez (1995, 2001) and Alarcón and Pinto (2015).

Previous geochronological and paleontological studies (Jordan et al., 1996; López et al., 2011), together with detrital zircon data described herein, show that the MFB developed during the early to late Miocene. Clast counts from the Conglomeratic Sandstone member that overlies the Las Hornillas breccia member (Fig. 16 in Alarcón and Pinto, 2015; data from Pérez, 2001) show a main contribution from the Choiyoi Magmatic Province and a minor contribution from Mesozoic sedimentary rocks (red sandstones and limestones). Based on variations in provenance, four stages in the development of the basin are recognized (ca. 22–19 Ma, ca. 19–16 Ma, ca. 16–10 Ma and ca. 10–8 Ma). Our data allow us to discuss the first three stages (ca. 22–10 Ma, Fig. 13).

6.4.1. Stage 1 (ca. 22–19 Ma): Provenance from the Principal Cordillera

The period between ca. 22 and 19 Ma, representing the earliest stage of the MFB (IQ-01 to PA-02, Fig. 5), was characterized by a significant contribution of detritus sourced from Oligo–Miocene volcanic rocks in the Principal Cordillera (Fig. 13A, B). Input from Miocene volcanics is revealed by the association of clinopyroxenes and amphiboles in samples LP-02, LP-01, IQ-02, IQ-01 and IQ-03 (Fig. 5, and Table S1 in Supplementary Material), whose geochemistry indicates calc-alkaline andesitic and andesitic-dacitic sources. This compositional character is consistent with the intermediate to basic signatures and porphyritic and trachytic textures of volcanic lithics recognized in sedimentary rocks in the lowest Chinches Formation, together with a low quantity of quartz (Fig. 5) (Alarcón and Pinto, 2015). Moreover, the detrital zircon peaks at ca. 22 and ca. 35 Ma (~52%, LP-01) and ca. 19, ca. 22, and ca. 41 Ma (~10%, IQ-01) support a Cenozoic contribution (Fig. 11A–B, and Table 1), probably corresponding to the Oligo–Miocene volcanic arc in the Principal Cordillera (e.g., Abanico and Farellones Formations, Laguna del Pelado Volcanic Complex, Mpodozis et al., 2009; Jara, 2013; Jara and Charrier, 2014) and igneous rocks associated to the Paleogene plutonic belt (Parada et al., 2007).

Permian–Triassic Choiyoi igneous rocks also supplied sediment at this stage (Fig. 13A) as indicated by a minor detrital zircon population (ca. 262 Ma, ~10%) in the upper Areniscas Chocolate member (sample LP-01) and the presence of rhyolitic clasts within the conglomerates at the basal part of the Areniscas Chocolate member (Mirré, 1966). The presence of material eroded from the Choiyoi Magmatic Province indicates that this unit was exposed as a minor source from the earliest stage of MFB development, prior to ca. 22 Ma.

The age of this period is constrained by detrital zircons ages of ca. 22 and ca. 19 Ma in strata immediately below and over the Las Hornillas volcanic breccia member, and also by the estimated age of this breccia (ca. 20 Ma, Pérez, 2001). The presence of the Las Hornillas breccia member also confirms synchronous volcanism at this time. Pérez (2001) correlated this breccia with the eastern Las Pichireguas volcanic breccia in the La Ramada Volcanic Complex and to the northern Barreal subvolcanic complex (Fig. 1C). However, the Las Pichireguas breccia has a different geochemical signature. The Las Hornillas breccia member is geochemically more similar to the La Laguna subvolcanic body, but is believed to be older (ca. 20 vs. ca. 15 Ma). More geochemical and mineralogical studies of volcanic and subvolcanic rocks are needed to establish correlations more clearly.

These results show the Principal Cordillera constituted a positive relief at ca. 22–19 Ma and would have supplied material to the MFB. This relief would have been produced by tectonic uplift related to the Río Mercedario Thrust (Fig. 3A), as proposed by Cristallini and Ramos (2000).

6.4.2. Stage 2 (ca. 19–16 Ma): Provenance from the westernmost Frontal Cordillera

In the period between ca. 19 and 16 Ma (IQ-01 to PA-02), above the Las Hornillas breccia member, supply from Cenozoic volcanic rocks diminished dramatically and the Choiyoi igneous rocks became the main source (Fig. 13B–C).

Significant contribution from the Choiyoi Magmatic Province is evidenced by the increase in the abundance of Permian–Triassic detrital zircon ages (ca. 256 Ma, ~71%) in sample IQ-01 compared with sample LP-01 (ca. 262 Ma, ~10%) (Fig. 11A–B, and Table 1). This supply is consistent with the abundance of rhyolitic clasts (Pérez, 2001) in this part of the succession (Fig. 5). The decrease in supply from Cenozoic sources is recorded by the reduction in the abundance of detrital zircon of these ages in sample IQ-01 (~10%) compared with sample LP-01 (~52%) (Fig. 11A–B, and Table 1). An associated change in heavy mineral assemblages is noticeably seen above sample IQ-03 (Fig. 5, and Table S1 in Supplementary Material), where the almost complete absence of clinopyroxene and amphibole supports an acidic igneous source.

The age of this period is given by maximum depositional ages of ca. 19 Ma in sample IQ-01, immediately above the Las Hornillas volcanic breccia member, and ca. 17 Ma in sample PA-02 from the fossiliferous lacustrine unit at ~1500 m, together with the age of ca. 16 Ma estimated by magnetostratigraphy (Jordan et al., 1996; Ruskin et al., 2011).

This change of provenance, involving exhumation of the Choiyoi

Magmatic Province, suggests tectonic uplift of the western Frontal Cordillera to the west of the MFB. According to the structural model of Cristallini and Ramos (2000), thrusting in the La Ramada fold-and-thrust belt was activated from west to east. The most probable thrust activated at this time would correspond to the La Ramada Thrust (Fig. 3A), which is the westernmost thrust to deform the Choiyoi Magmatic Province at this latitude (Fig. 3A–B). Furthermore, the La Ramada Thrust is sealed by the La Ramada Volcanic Complex, the oldest reported age of which is ca. 13 Ma (Pérez and Ramos, 1996), which is consistent with a prior thrust activation at ca. 19 Ma.

6.4.3. Stage 3 (ca. 16–10 Ma): Provenance from the Principal and Frontal Cordilleras

In the period between ca. 16 and 10 Ma (PA-02 to MA-10), the Choiyoi Magmatic Province continued to be a significant contributor to the MFB, but Cenozoic volcanics once again became a significant sediment source (Fig. 13D). The Choiyoi Magmatic Province source is recorded by detrital zircon age peaks at ca. 252 and ca. 270 Ma (~45%, sample PA-02) and ca. 250 Ma (~59%, sample MA-10) (Table 1). This supply is supported by the presence of rhyolitic clasts in the conglomerates (Pérez, 2001) (Fig. 4).

The volcanic source is evidenced by a substantial increase in abundance of clinopyroxenes and amphiboles from samples PA-03 to MA-05 (Fig. 5, Table S1 in Supplementary Material), and also by the Cenozoic ages of detrital zircons, ca. 17 and ca. 49 Ma (PA-02, ~9%) and ca. 15 Ma (MA-10, ~15%) (Fig. 11C–D, and Table 1). The volcanic source is mainly calc-alkaline continental (MA-01 to MA-05), with calc-alkaline island arc in some strata (MA-06 to MA-10) (Figs. 5 and 9C). The calc-alkaline continental source probably corresponds to the Farellones Formation, which has a similar geochemical signature (e.g., Nyström et al., 2003). Moreover, the Paleogene detrital zircon ages indicate erosion of igneous rocks from the Paleogene plutonic belt. Thus, at this stage the Principal Cordillera to the west was again captured by the paleodrainage system and became a source to the MFB.

We propose that the calc-alkaline island arc source corresponds to the La Ramada Volcanic Complex and La Laguna Andesite, which developed in a back-arc position in the Cordón de la Ramada and Cordón del Espinacito (Fig. 3). This proposal is supported by the 15.45 ± 0.30 Ma age (Ar–Ar, Pérez and Ramos, 1996) reported for the La Laguna Andesite, which is similar to detrital zircon ages from the upper Chinches Formation (ca. 15 Ma, MA-10). Moreover, the La Ramada Volcanic Complex is characterized by hornblende-bearing andesites, which could have contributed the magnesio-hornblendes to the upper Chinches Formation (MA-06 to MA-10). The scarcity of clinopyroxene and progressive increase in amphibole at the top of the upper unit (MA-06 to MA-10) (Fig. 5) could reflect this local volcanic source. Furthermore, the approximate age of these strata (< 10 Ma, ~3000–3100 m, Fig. 5) is consistent with the age of the La Ramada Volcanic Complex (ca. 13–11 Ma) in terms of a potential source of rocks.

The age of this period is given by the magnetostratigraphic ages of lacustrine deposits at ~1500 m (ca. 15.7 Ma) and ~2800 m (ca. 9.74 Ma) (Ruskin et al., 2011). Maximum depositional ages of ca. 17 Ma (PA-02) and ca. 15 Ma (MA-10) evidenced by detrital zircons are consistent but slightly older than the magnetostratigraphic ages (Fig. 12).

Thus, during this stage, both the Principal Cordillera and the western Frontal Cordillera were eroded. The location of the Miocene volcanic and subvolcanic sources (La Ramada Volcanic Complex and the La Laguna Andesite) covering the La Ramada Thrust and to the east of the El Espinacito Thrust (Fig. 3A), suggests activity of the El Espinacito Thrust post–10 Ma. This interpretation is consistent with the normal sequence of thrusting proposed by Cristallini and Ramos (2000).

6.5. Regional paleogeographic and tectonic implications

The age of the Frontal Cordillera uplift is crucial to understand the tectonic evolution of the upper crustal deformation in the studied segment, considering that this range was developed as part of an Andean fold-and-thrust belt (e.g., Cristallini and Ramos, 2000). It has been proposed that this morphostructural range developed diachronously from north to south (e.g., Giambiagi et al., 2003). However, our results and analysis allow us to propose an alternative explanation for the differences in the timing of the Frontal Cordillera uplift. Next, we explain how the Frontal Cordillera developed by mean of two diachronous thick-skinned scales, the La Ramada–Espinacito ranges at ca. 19–12 Ma, followed by the Cordillera del Tigre at ca. 12–11 Ma, coeval with the uplifting of first scales in the Precordillera. We also discuss correlations of the uplift of the Frontal Cordillera to the north and to the south, and we discuss how this evolution explains the history of connectivity of the MFB with other Neogene basins in the Precordillera region.

6.5.1. Low paleorelief in the Frontal Cordillera region (> 22 Ma)

Our data indicate that at ca. 22 Ma, the Frontal Cordillera at ~31.5°–32.5°S constitutes a low positive paleorelief, supplying few materials to the basin. This is consistent with the onset of Frontal Cordillera uplift at ca. 25–24 Ma proposed by Levina et al. (2014) based on provenance studies in the Precordillera deposits at these latitudes. Between ca. 22 and 19 Ma, the Principal Cordillera fed the foreland basins to the east. Proximal foreland basins, such as the MFB, developed next to the Principal Cordillera and extended into the Precordillera region as distal foreland environments, with fluvial–eolian deposits found in Riquiliponche (Reyna et al., 2010), Pachaco and Talacasto (Levina et al., 2014) (Fig. 3), which correlate with the Areniscas Chocolate member of the Chinches Formation. Similar facies in the basal parts of stratigraphic successions in the Precordillera at ~30°–31°S, such as the Caracol and Río Blanco valleys and Los Blanquitos sections (Jordan et al., 1993) (Fig. 2), can also be correlated with this part of the foreland evolution.

6.5.2. Western Crontal Cordillera uplift (ca. 19 Ma)

The western Frontal Cordillera, equivalent to the La Ramada–Espinacito ranges (Figs. 1, 2 and 3), was significantly uplifted at ca. 19 Ma, leading to influx of rhyolitic material from the Choiyoi Magmatic Province to the proximal MFB and distal deposits, such as found in the Pachaco and Talacasto basin segments in the Precordillera region (Levina et al., 2014) (Fig. 2). It is uncertain when this western block of the Frontal Cordillera stopped supplying detritus to the Precordillera region, but Permo–Triassic rhyolitic clasts and tuffaceous deposits of ca. 15 Ma (Ar–Ar, Bercowski et al., 1993) intercalated in sedimentary deposits in the La Chilca sector (easternmost Central precordillera, Fig. 2) suggest that the western Frontal Cordillera fed this area until at least the middle Miocene.

6.5.3. Eastern Frontal Cordillera uplift (ca. 12 Ma)

The uplift of the eastern Frontal Cordillera is less evident in its northern part at the study latitude (Cordillera del Tigre, Figs. 1C, 2A and 3). The paleocurrents in the MFB, on its eastern side, registered contribution from the east post–10 Ma (Fig. 5), suggesting a supply from the Cordillera del Tigre. However, since the Cordillera del Tigre is formed by the Choiyoi Magmatic Province similar to the Cordón del Espinacito, it is impossible to determine its real contribution to the basin. On the eastern side of the Cordillera del Tigre, the Uspallata Basin has ages between ca. 12 and 8 Ma (Cortés et al., 1993; Hoke et al., 2014; Mahoney et al., 2014), contemporaneous to the upper Chinches Formation. Cortés et al. (1994) proposed the Uspallata Basin is an intermontane depression developed between the Cordillera del Tigre and the Precordillera, which suggests uplift of these ranges from at least from ca. 12 Ma. The onset of exhumation of the Cordón del Plata, which

is the prolongation to the south of the Cordillera del Tigre (~33°S, Fig. 2A), is well constrained to ca. 11.7–9.0 Ma by the La Pilona Formation (Irigoyen et al., 2000). To the east, in the Sierra de Las Peñas, the onset of Precordillera exhumation is evidenced by early Paleozoic detrital zircons ages within the La Pilona Formation (Iverson et al., 2012). The age of this formation, ca. 9–8 Ma (U–Pb, Iverson et al., 2012), is consistent with the age of the upper Uspallata Basin. These data constrain the beginning of the Cordillera del Tigre uplift to ca. 12 Ma (Fig. 13D). The uplift of this eastern part of the Frontal Cordillera suggests the MFB developed as a proximal foredeep during > 22–12 Ma and transformed to a piggyback basin or a broken foreland basin at ca. 12 Ma (according to Strecker et al., 2011). The thick-skinned behavior of the Cordillera del Tigre, and the probable synchronicity of uplift starting of the Cordillera del Tigre and the Precordillera support a broken foreland basin for the MFB for the stage > 12 Ma, as has been suggested by Hoke et al. (2015).

6.5.4. Correlations of Frontal Cordillera uplift to the north and to the south

To the north (~29°–30°S), it has been proposed that Frontal Cordillera uplift started at ca. 18–13 Ma (e.g., Winocur et al., 2015; Rossel et al., 2016; Suriano et al., 2017). In this area, the basal part of the sedimentary succession in the Iglesia Basin could be equivalent to the lower Chinches Formation (Fig. 2B) (17.2 ± 3.8 Ma, Jordan et al., 1997; Ré et al., 2003) and thus could represent the onset of the Frontal Cordillera uplift as a morphostructure at ~30°S. A more precise age of these deposits could help to establish correlations with the southern basins. The Frontal Cordillera at ~30°S seems to be related to the western Frontal Cordillera at ~32°15′S, and to be equivalent to the Cordón de La Ramada and the Cordón del Espinacito (Figs. 1C and 2A). In this case, the Frontal Cordillera at ~30°S developed between ca. 19 and 12 Ma, as in the Manantiales area. This proposal is consistent with the important shift in sediment provenance established by Fosdick et al. (2015) at 30°S based on detrital zircon ages, which showed a substantial decrease in Permo–Triassic Choiyoi age zircons (Frontal Cordillera) between ca. 12 and ca. 10 Ma, and dominance of Carboniferous–Permian zircons (Precordillera) from ca. 10 to to 8 Ma.

To the south, at ~33°–34°S, Giambiagi et al. (2016) and Porras et al. (2016) established that the Frontal Cordillera developed from ca. 12–11 Ma. However, the uplifted block of the Frontal Cordillera at these latitudes (Cordón del Plata–Cordón del Portillo, Fig. 1C) is geographically equivalent only to the eastern Frontal Cordillera at ~31.5°–32.5°S (Cordillera del Tigre), implying the uplift of the Cordillera del Tigre, the Cordón del Plata and the Cordón del Portillo are coeval (ca. 12–11 Ma).

7. Conclusions

U–Pb ages of detrital zircons from the lower Chinches Formation indicate that the MFB began to develop at least from ca. 22 Ma. Provenance analysis of the basin succession provides evidence for two separate pulses of Miocene volcanic detritus to the MFB, at ca. 19 and ca. 16 Ma. These source rocks were mainly of calc-alkaline intermediate character, and probably correspond to the early Miocene Farellones Formation (Principal Cordillera), and the middle Miocene La Ramada Volcanic Complex and La Laguna Andesite (Frontal Cordillera). The Permian–Triassic Choiyoi Magmatic Province was a low paleorelief at the beginning of the MFB, with Cenozoic volcanic and plutonic rocks being the most significant contributor at around 22–19 Ma. At ca. 19 Ma there was a marked change in provenance, with the Choiyoi Magmatic Province becoming the dominant source of sediment for the MFB during the rest of its evolution. This change is probably related to the tectonic uplift of western blocks of the Frontal Cordillera by the activation of the La Ramada thrust of the La Ramada fold-and-thrust belt. At ca. 16 Ma the Cenozoic igneous source was again registered, corresponding to a mixture of volcanic, subvolcanic and plutonic rocks from the Principal Cordillera and western Frontal Cordillera by the activation in normal sequence of the Espinacito thrust of the La Ramada fold-and-thrust belt. The foreland character of the MFB with distal supply to the Precordillera remained until ca. 12 Ma when the eastern Frontal Cordillera (Cordillera del Tigre) was uplifted, and the MFB was probably cut off from the eastern area, becoming a broken foreland basin. Therefore, the Frontal Cordillera was developed with two diachronous N-S thick-skinned blocks from west to east. The first one is equivalent to uplifted blocks that contributed to Miocene eastern basins at ~30°–32°S, and the second one coeval to the beginning of the Precordillera uplift. Mesoproterozoic–Devonian detrital zircons registered in the basin probably represent recycled material from Mesozoic sedimentary units from the Principal Cordillera.

Supplementary data to this article can be found online at https://doi.org/10.1016/j.palaeo.2017.12.017.

Acknowledgments

We are grateful for funding via the Fondecyt Project 1090165 (Luisa Pinto). Significant support was obtained from the IGCP-586Y Project, which supported the field trips and scientific meetings and helped us to improve our interpretations. We also appreciate the support given by the Geology Department of the Universidad de Chile. Important scientific contributions were made through collaborations with B. Mahoney (University of Wisconsin-Eau Claire), B. Moine (CNRS, France), G. Hoke (Syracuse University, United States) and L. Giambiagi (CONICET, Argentina). We thank the researchers V. Valencia (Valencia Geoservices) and L. Solari (Universidad Nacional Autónoma de México), who carried out the geochronological datings, and G. Turner (British Geological Survey), who undertook the mineral chemical analysis. We thank K. Deckart (Universidad de Chile), J. Flynn (American Museum of Natural History), J. Suriano (Universidad de Buenos Aires, CONICET), R. Palermo (Earth, Atmospheric and Planetary Sciences, Massachusetts Institute of Technology), and J. Hu (University of Illinois) for their help and interesting discussions. Special thanks are due to S. Herrera, H.Rivera (Universidad de Chile), R. Charrier (Universidad de Chile, Universidad Andres Bello), H. Bahlburg (University of Münster), and an anonymous referee, who carefully reviewed our manuscript and whose comments enabled us to improve it. Finally, we appreciate the technical assistance provided by J. Vargas (Universidad de Chile), M. Olivera of Don Lisandro (Barreal, Argentina) and we would like to thank the staff at X-Strata (La Junta, Argentina) for their logistical support in the field campaigns.

References

Aguirre, L., Calderón, S., Vergara, M., Oliveros, V., Morata, D., Belmar, M., 2009. Edades isotópicas de rocas de los valles Volcán y Tinguiririca, Chile central. In: 12th Congreso Geológico Chileno, Santiago, Servicio Nacional de Geología y Minería. Actas S8-001, Digital, (4 p).

Alarcón, P., Pinto, L., 2015. Neogene erosion of the Andean cordillera in the flat-slab segment as indicated by petrography and whole-rock geochemistry from the Manantiales Foreland Basin (32°–32°30′S). Tectonophysics 639, 1–22. http://dx.doi.org/10.1016/j.tecto.2014.11.001.

Álvarez, P.P., Benoit, S.V., Ottone, E.G., 1995. Las Formaciones Rancho de Lata, Los Patillos y otras unidades mesozoicas de la Alta Cordillera Principal de San Juan. Rev. Asoc. Geol. Argent. 50 (1–4), 123–142.

Álvarez, J., Mpodozis, C., Arriagada, C., Astini, R., Morata, D., Salazar, E., Valencia, V.A., Vervoort, J.D., 2011. Detrital zircons from late Paleozoic accretionary complexes in north–central Chile (28°–32°S): possible fingerprints of the Chilenia terrane. J. S. Am. Earth Sci. 32, 460–476.

Bahlburg, H., Vervoort, J.D., Du Frane, S.A., Bock, B., Augustsson, C., Reimann, C., 2009. Timing of crust formation and recycling in accretionary orogens: insights learned from the western margin of South America. Earth Sci. Rev. 97, 215–241.

Balgord, E.A., Carrapa, B., 2016. Basin evolution of upper cretaceous–lower Cenozoic strata in the Malargüe fold-and-thrust belt: northern Neuquén Basin, Argentina. Basin Res. 28, 183–206. http://dx.doi.org/10.1111/bre.12106.

Bercowski, F., Ruzycki, L., Jordan, T., Zeitler, P., Caballero, M.M., Perez, I., 1993. Litofacies y edad isotópica de la secuencia La Chilca y su significado paleogeográfico para el Neógeno de Precordillera. In: 12th Congreso Geológico Argentino and 2nd Congreso de Exploración de Hidrocarburos, Proceedings T°1, pp. 212–217.

Boyce, D., 2015. Modelo de evolución tectónica y paleogeográfica del margen andino en Chile Central durante el cretácico medio - tardío: El registro estructural y

sedimentario en la formación Las Chilcas (M.Sc. Thesis). Departamento de Geología, Universidad de Chile (296 pp).
Brennan, P.R.K., Ridgway, K.D., 2015. Detrital zircon record of Neogene exhumation of the central Alaska range: a far-field upper plate response to flat-slab subduction. Geol. Soc. Am. Bull. 127 (7/8), 945–961. http://dx.doi.org/10.1130/B31164.1.
Buelow, E., Suriano, J., Mahoney, J.B., Mescua, J., Giambiaggi, L., Kimbrough, D., Rieners, P., 2014. Stratigraphic analysis of the Neogene Cachueta Basin: A record of orogenic exhumation and basin inversion in the south central Andes. In: Geological Society of America Meeting, 19–22 October, Vancouver, Canada, Poster, N°143-10.
Carrapa, B., Trimble, J.D., Stockli, D.F., 2011. Patterns and timing of exhumation and deformation in the Eastern Cordillera of NW Argentina revealed by (U-Th)/He thermochronology. Tectonics 30, TC3003 https://doi.org/10.1029/2010TC002707.
Carrapa, B., Bywater-Reyes, S., DeCelles, P.G., Mortimer, E., Gehrels, G.E., 2012. Late Eocene-Pliocene basin evolution in the Eastern Cordillera of northwestern Argentina (25°-26°S): Regional implications for Andean orogenic wedge development. Basin Res. 24, 249–268.
Carmichael, I.S.E., Nicholls, J., Smith, L., 1970. Silica activity in igneous rocks. Am. Mineral. 55, 246–263.
Cawood, P.A., Nemchin, A.A., Strachan, R.A., Prave, A.R., Krabbendam, M., 2007. Sedimentary basin and detrital zircon record along east Laurentia and Baltica during assembly and breakup of Rodinia. J. Geol. Soc. 164, 257–275. http://dx.doi.org/10.1144/0016-76492006-115.
Charrier, R., Baeza, O., Elgueta, S., Flynn, J., Gans, R., Kay, S., Muñoz, N., Wyss, A., Zurita, E., 2002. Evidence for Cenozoic extensional basin development and tectonic inversion south of the flat-slab segment, southern Central Andes, Chile (33°–36°S). J. S. Am. Earth Sci. 15, 117–139.
Charrier, R., Pinto, L., Rodríguez, M.P., 2007. Tectonostratigraphic evolution of the Andean orogen in Chile. In: Moreno, T., Gibbons, W. (Eds.), The Geology of Chile. Vol. 3. Geological Society of London, Special Publication, pp. 21–114.
Cortés, J.M., 1993. El frente de corrimiento de la Cordillera Frontal y el extremo sur del valle de Uspallata, Mendoza. Ramos, V. (Ed.), 12th Congreso Geológico Argentino y 2nd Congreso de Exploración de Hidrocarbouros, Proceedings 168–178 Buenos Aires, Argentina.
Cortés, J., 1994. La segmentación tectónica de la Depresión de Uspallata, Mendoza, Argentina. 7th Congreso Geológico Argentino 1. Proceedings, Concepción, Chile, pp. 18–22.
Cristallini, E.O., Cangini, A.H., 1993. Estratigrafía y estructuras las nacientes del río Volcan, Alta Cordillera de San Juan. In: 2nd Congreso Geológico Argentino, and 12th Congreso de Exploración de Hidrocarburos, Proceedings, Buenos Aires, Argentina. Vol. 3. pp. 85–92.
Cristallini, E.O., Ramos, V.A., 2000. Thick-skinned and thin-skinned thrusting in La Ramada fold and thrust belt. Crustal evolution of the high Andes of San Juan, Argentina (32° SL). Tectonophysics 317, 205–235.
Cristallini, E.O., Mosquera, A., Ramos, V.A., 1994. Estructura de la Alta Cordillera de San Juan. Rev. Asoc. Geol. Argent. 49 (1–2), 165–183.
Cristallini, E., Álvarez, P., Pérez, D., Ramos, V., 1996. Carta Geológica de la región de La Ramada. Servicio Geológico Nacional, 1 map, scale 1:100,000, Argentina.
DeCelles, P.G., Giles, K.A., 1996. Foreland basin systems. Basin Res. 8 (2), 105–123.
Deer, W.A., Howie, R.A., Zussman, J., 1962. An Introduction to the Rock-Forming Minerals. Longmans, London (528 p).
Deer, W.A., Howie, R.A., Zussman, J., 1997. Rock-Forming Minerals, Volume 1A: Orthosilicates, 2nd ed. Geological Society of London (919 pp).
Dutrow, B., Henry, D.J., 2000. Complexly zoned fibrous tourmaline: a record of evolving magmatic and hydrothermal fluids. Can. Mineral. 38, 131–143.
Fedo, C.M., Sircombe, K.N., Rainbird, R.H., 2003. Detrital zircon analysis of the sedimentary record. In: Hanchar, J.M., Hoskin, P.W.O. (Eds.), Zircon, Reviews in Mineralogy and Geochemistry. Vol. 53. Mineralogical Society of America, Washington DC, pp. 277–303.
Flynn, J.J., Swisher III, C.C., 1995. Cenozoic South American Land Mammal Ages: Correlation to Global Geochronologies. In: Berggren, W.A., Kent, D.V., Aubry, M.-P., Hardenbol, J. (Eds.), Geochronology, Time Scales and Global Stratigraphic Correlation, Special Publication. Vol. 54. SEPM (Society of Sedimentary Geology), Tulsa, pp. 317–333.
Flynn, J.J., Charrier, R., Croft, D.A., Wyss, A.R., 2012. Cenozoic Andean Faunas: Shedding New Light on South American Mammal Evolution, Biogeography, Environments, and Tectonics. In: Patterson, B.D., Costa, L.P. (Eds.), Bones, Clones, and Biomes: The History and Geography of Recent Neotropical Mammals. University of Chicago Press, pp. 51–75.
Fosdick, J.C., Carrapa, B., Ortíz, G., 2015. Faulting and erosion in the argentine Precordillera during changes in subduction regime: reconciling bedrock cooling and detrital records. Earth Planet. Sci. Lett. 432, 73–83. http://dx.doi.org/10.1016/j.epsl.2015.09.041.
Fosdick, J.C., Reat, E.J., Carrapa, B., Ortiz, G., Alvarado, P.M., 2017. Retroarc basin reorganization and aridification during Paleogene uplift of the southern central Andes. Tectonics 36, 493–514. http://dx.doi.org/10.1002/2016TC004400.
Gans, C.R., Beck, S.L., Zandt, G., Gilbert, H., Alvarado, P., Anderson, M., Linkimer, L., 2011. Continental and oceanic crustal structure of the Pampean flat slab region, western Argentina, using receiver function analysis: new high-resolution results. Geophys. J. Int. 186 (1), 45–58.
Gehrels, G.E., 2014. Detrital zircon U-Pb geochronology applied to tectonics. Annu. Rev. Earth Planet. Sci. 42, 127–149.
Giambiagi, L.B., Álvarez, P.P., Godoy, E., Ramos, V.A., 2003. The control of pre-existing extensional structures in the evolution of the southern sector of the Aconcagua fold and thrust belt. Tectonophysics 369, 1–19.
Giambiagi, L., Mescua, J., Bechis, F., Hoke, G., Suriano, J., Spagnotto, S., Moreiras, S.M., Lossada, A., Mazzitelli, M., Toural Dapoza, R., Folguera, A., Mardonez, D., Pagano, D.S., 2016. Cenozoic orogenic evolution of the southern Central Andes (32–36°S). In: Folguera, A. (Ed.), Growth of the Southern Andes. Springer Earth System Sciences, pp. 63–98. http://dx.doi.org/10.1007/978-3-319-23060-3_4.
Gutscher, M.A., Spakman, W., Bijwaard, H., Engdahl, E.R., 2000. Geodynamics of flat subduction: seismicity and tomographic constraints from the Andean margin. Tectonics 19 (5), 814–833.
Hawthorne, F.C., Oberti, R., Harlow, G.E., Maresch, W.V., Martin, R.F., Schumacher, J.C., Welch, M.D., 2012. Nomenclature of the amphibole supergroup. Am. Mineral. 97, 2031–2048.
Hayes, G.P., Wald, D.J., Johnson, R.L., 2012. Slab1.0: a three-dimensional model of global subduction zone geometries. J. Geophys. Res. Solid Earth 117 (1978–2012), B1.
Henry, D.J., Dutrow, B.L., 1996. Metamorphic tourmaline and its petrologic applications. In: Grew, E.S., Anovitz, L.M. (Eds.), Boron: Mineralogy, Petrology and Geochemistry. Reviews in Mineralogy Vol. 33. Mineralogical Society of America, pp. 503–557.
Henry, D., Guidotti, C., 1985. Tourmaline as a petrogenetic indicator mineral: an example from the staurolite-grade metapelites of NW Maine. Am. Mineral. 70, 1–15.
Henry, D.J., Novák, M., Hawthorne, F.C., Ertl, A., Dutrow, B.L., Uher, P., Pezzotta, F., 2011. Nomenclature of the tourmaline supergroup-minerals. Am. Mineral. 96, 895–913.
Hoke, G.D., Giambiagi, L.B., Garzione, C.N., Mahoney, J.B., Strecker, M.R., 2014. Neogene paleoelevation of intermontane basins in a narrow, compressional mountain range, southern Central Andes of Argentina. Earth Planet. Sci. Lett. 406, 153–164.
Hoke, G.D., Graber, N.R., Mescua, J.F., Giambiagi, L.B., Fitzgerald, P.G., Metcalf, J.R., 2015. Near Pure Surface Uplift of the Argentine Frontal Cordillera: Insights From (U–Th)/He Thermochronometry and Geomorphic Analysis. Vol. 399. Geological Society, London, Special Publications, pp. 383–399. http://dx.doi.org/10.1144/SP399.4.
Hu, J., Liu, L., Hermosillo, A., Zhou, Q., 2016. Simulation of late Cenozoic south American flat-slab subduction using geodynamic models with data assimilation. Earth Planet. Sci. Lett. 438, 1–13.
Iglesia Llanos, M.P., 1995. Geología del área de Manantiales al este del cordón del Espinacito, Provincia de San Juan. Rev. Asoc. Geol. Argent. 50 (1–4), 195–211.
Irigoyen, M.V., Buchan, K.L., Brown, R.L., 2000. Magnetostratigraphy of Neogene Andean foreland-basin strata, lat 33°S, Mendoza Province, Argentina. Geol. Soc. Am. Bull. 112 (6), 803–816.
Iverson, O.R., Mahoney, J.B., Benusa, K.M., Kimbrough, D., 2012. Neogene basin evolution in the Las Penas Basin, Salagasta Region, Mendoza, Argentina. In: 64th Geological Society of America, Proceedings, 9–11 May, Rocky Mountain Section. Vol. 44 (6). pp. 92.
Jakes, P., White, A.J.R., 1972. Hornblendes from calc-alkaline volcanic rocks of island arcs and continental margins. Am. Mineral. 57, 887–902.
Jara, P., 2013. Tectónica mezo-cenozoica en la Cordillera Principal de Chile central entre 32° y 33°S. In: Análisis a partir de nuevos antecedentes de campo y modelamiento analógico. Universidad de Chile, Chile (PhD Thesis). (249 pp).
Jara, P., Charrier, R., 2014. Nuevos antecedentes estratigráficos y geocronológicos para el Meso–Cenozoico de la Cordillera Principal de Chile entre 32° y 32°30´S. Implicancias estructurales y paleogeográficas. Andean Geol. 41 (1), 174–209. http://dx.doi.org/10.5027/andgeoV41n1-a07.
Jordan, T., 1995. Retroarc foreland and related basins. In: Busby, C., Ingersoll, R. (Eds.), Tectonics of Sedimentary Basins. Blackwell, Boston, pp. 331–362.
Jordan, T.E., Isacks, B.L., Allmendinger, R.W., Brewer, J.A., Ramos, V.A., Ando, C.J., 1983. Andean tectonics related to geometry of subducted Nazca plate. Geol. Soc. Am. Bull. 94, 341–361.
Jordan, T.E., Allmendinger, R.W., Damanti, J.F., Drake, R.E., 1993. Chronology of motion in a complete Thrust Belt: the Precordillera, 30–31°S, Andes Mountains. J. Geol. 101, 135–156.
Jordan, T.E., Tamm, V., Figueroa, G., Flemings, P.B., Richards, D., Tabbutt, K., Cheatham, T., 1996. Development of the Miocene Manantiales foreland basin, principal cordillera, San Juan, Argentina. Rev. Geol. Chile 23 (1), 43–79.
Jordan, T.E., Kelly, S., Fernández, A., Fernández Seveso, F., Ré, G.H., Milana, J.P., 1997. Relaciones entre las historias evolutivas de las cuencas de Iglesia y Bermejo, Provincia de San Juan, Argentina. 2nd Jornadas de Geología de Precordillera Proceedings, San Juan, Argentina, pp. 142–147.
Krawinkel, H., Wozazek, S., Krawinkel, J., Hellmann, W., 1999. Heavy-mineral analysis and clinopyroxene geochemistry applied to provenance analysis of lithic sandstones from the Azuero–Soná complex (NW Panama). Sediment. Geol. 124, 149–168.
Krippner, A., Meinhold, G., Morton, A., von Eynatten, H., 2014. Evaluation of garnet discrimination diagrams using geochemical data of garnets derived from various host rocks. Sediment. Geol. 306, 36–52.
Le Bas, M., 1962. The role of aluminium in igneous clinopyroxenes with relation to their parentage. Am. J. Sci. 260, 267–288.
Leake, B.E., 1965. The relationship between tetrahedral aluminum and the maximum possible octohedral aluminum in natural calciferous and subcalciferous amphiboles. Am. Mineral. 50, 843–851.
Leake, B.E., Woolley, A., Arps, C., Birch, W., Gilbert, M., Grice, J., Hawthorne, F., Kato, A., Kisch, H., Krivovichev, V., Linthout, K., Laird, J., Mandarino, J., Maresch, W., Nickel, E., Rock, N., Schumacher, J., Smith, D., Stephenson, N., Ungaretti, L., Whittaker, E., Youzhi, G., 1997. Nomenclature of amphiboles: report of the Subcommitee on amphiboles of the international mineralogical association, commission on new minerals and mineral names. Am. Mineral. 82, 1019–1037.
Leake, B.E., Woolley, A.R., Birch, W.D., Burke, E.A.J., Ferraris, G., Grice, J.D., Hawthorne, F.C., Kisch, H.J., Krivovichev, V.G., Schumacher, J.C., Stephenson, N.C.N., Whittaker, E.J.W., 2004. Nomenclature of amphiboles: additions and revisions to the international mineralogical Association's amphibole nomenclature. Am. Mineral. 89, 883–887.

Leterrier, J., Maury, R.C., Thonon, P., Girard, D., Marchal, M., 1982. Clinopyroxene composition as a method of identification of the magmatic affinities of paleo-volcanic series. Earth Planet. Sci. Lett. 59, 139–154.
Leveratto, M.A., 1976. Edad de intrusivos cenozoicos en la Precordillera de San Juan y su implicancia estratigráfica. Rev. Asoc. Geol. Argent. 31, 53–88.
Levina, M., Horton, B.K., Fuentes, F., Stockli, D.F., 2014. Cenozoic sedimentation and exhumation of the foreland basin system preserved in the Precordillera thrust belt (31–32°S), southern central Andes, Argentina. Tectonics 33, 1659–1680. http://dx.doi.org/10.1002/2013TC003424.
López, G.M., Vucetich, M.G., Carlini, A.A., Bond, M., Pérez, M.E., Ciancio, M.R., Pérez, D.J., Arnal, M., Olivares, A., 2011. New Miocene mammal assemblages from Neogene Manantiales basin, Cordillera Frontal, San Juan, Argentina. In: Salfity, J.A., Marquillas, R.A. (Eds.), Cenozoic Geology of the Central Andes of Argentina. SCS Publisher, Salta, 978-987-26890-0-1, pp. 211–226.
Mahoney, J.B., Kimbrough, D., Hoke, G., Mescua, J., Giambiagi, L., Buelow, E., Hutter, A., Leidel, A., 2014. Cuenca Uspallata: An intermontane basin records episodic uplift of the Cordillera Frontal and Precordillera in the Late Miocene. In: Geological Society of America Meeting, 19–22 October, Vancouver, Canada, Poster, N°143-8.
Mange, M.A., Maurer, H.F.W., 1992. In: Hall & Chapman (Ed.), Heavy Minerals in Colour, 147 pp.
Mange, M.A., Morton, A.C., 2007. Geochemistry of heavy minerals. In: Mange, M., Wright, D.K. (Eds.), Heavy Minerals in Use. Developments in Sedimentology. Vol. 58. pp. 345–391.
Mange, M., Wright, D.K., 2007. Heavy Minerals in Use. Developments in Sedimentology. Vol. 58 Elsevier (1328 pp).
Martinod, J., Husson, L., Roperch, P., Guillaume, B., Espurt, N., 2010. Horizontal subduction zones, convergence velocity and the building of the Andes. Earth Planet. Sci. Lett. 299 (3–4), 299–309. http://dx.doi.org/10.1016/j.epsl.2010.09.010.
Mazzitelli, M.A., Mahoney, B., Balgord, E., Giambiagi, L., Kimbrough, D., Lossada, A., Mccann, C., 2015. Evolution of the Manantiales Basin, San Juan: Constraining miocene orogenic patterns in the South-Central Andes. In: Geological Society of America Meeting, 1–4 November, Maryland, USA. Vol. 47 (7). pp. 151 (Poster N°46-36).
Méres, S., 2008. Garnets–Important information resource about source area and parental rocks of the siliciclasic sedimentary rocks. In: Jurcovic, L. (Ed.), Conference "Cambelove dni 2008". Bratislava: Comenius University, Abstract Book, pp. 37–43.
Mirré, J.C., 1966. Geología del valle del Río de Los Patos (entre Barreal y Las Hornillas). Rev. Asoc. Geol. Argent. 21 (4), 211–231.
Morimoto, N., 1988. Nomenclature of pyroxenes. Mineral. Mag. 52, 535–550.
Morton, A.C., Allen, M., Simmons, M., Spathopoulos, F., Still, J., Hinds, D., Ismail-Zadeh, A., Kroonenberg, S., 2003. Provenance patterns in a neotectonic basin: Pliocene and quaternary sediment supply to the South Caspian. Basin Res. 15, 321–337.
Mpodozis, C., Brockway, H., Marquardt, C., Perelló, J., 2009. Geocronología U/Pb y tectónica de la región Los Pelambres–Cerro Mercedario: Implicancias para la evolución cenozoica de los Andes del centro de Chile y Argentina. In: 12th Congreso Geológico Chileno, Proceedings, Santiago, Chile, S9, N°59.
Mueller, P.A., Heatherington, A.L., Wooden, J.L., Shuster, R.D., Nutman, A.P., Williams, I.S., 1994. Precambrian zircons from the Florida basement: a Gondwana connection. Geology 22, 119–122.
Muñoz-Sáez, C., Pinto, L., Charrier, R., Nalpas, T., 2014. Influence of depositional load on the development of a shortcut fault system during the inversion of an extensional basin: the Eocene–Oligocene Abanico Basin case, central Chile Andes (33°–35°S). Andean Geol. 41 (1), 1–28. http://dx.doi.org/10.5027/andgeoV41n1-a01.
Naipauer, M., Vujovich, G., Cingolani, C.A., McClelland, W.C., 2010. Detrital zircon analysis from the Neoproterozoic–Cambrian sedimentary cover (Cuyania terrane), sierra de Pie de Palo, Argentina: evidence of a rift and passive margin system? J. S. Am. Earth Sci. 29, 306–326.
Nechaev, V.P., 1991. Evolution of the Philippine and Japan seas from the clastic sediment record. Mar. Geol. 97, 167–190.
Nechaev, V.P., Isphording, W.P., 1993. Heavy mineral assemblages of continental margin as indicators of plate tectonic environments. J. Sediment. Petrol. 63, 1110–1117.
Nyström, J.O., Vergara, M., Morata, D., Levi, B., 2003. Tertiary volcanism during extension in the Andean foothills of central Chile (33°15′–33°45′S). Geol. Soc. Am. Bull. 115, 1523–1537.
Ogg, J.G., Smith, A.G., 2004. A geomagnetic polarity time scale. In: Gradstein, F.M., Ogg, J.G., Smith, A.G. (Eds.), A Geologic Time Scale 2004. Cambridge University Press, Cambridge.
Oliveros, V., Labbe, M., Rossel, P., Charrier, R., Encinas, A., 2012. Late Jurassic paleogeographic evolution of the Andean back-arc basin: new constrains from the Lagunillas formation, northern Chile (27°30′–28°30′S). J. S. Am. Earth Sci. 37, 25–40.
Parada, M.A., López-Escobar, L., Oliveros, V., Fuentes, F., Morata, D., Calderón, M., Aguirre, L., Féraud, G., Espinoza, F., Moreno, H., Figueroa, O., Muñoz Ravo, J., Troncoso Vásquez, R., Stern, C.R., 2007. Andean magmatism. In: Moreno, T., Gibbons, W. (Eds.), The Geology of Chile. Vol. 3. Geological Society of London, Special Publication, pp. 115–146.
Parfenoff, A., Pomerol, C., Tourenq, J., 1970. In: et Cie, Masson (Ed.), Les minéraux en grains. Méthodes d'étude et de détermination Paris, 578 pp.
Pérez, D.J., 1995. Estudio geológico del Cordón del Espinacito y regiones adyacentes, provincial de San Juan (PhD Thesis). Universidad de Buenos Aires, Argentina (262 pp).
Pérez, D.J., 2001. Tectonic and unroofing history of Neogene Manantiales foreland basin deposits, cordillera frontal (32°30´S), San Juan Province, Argentina. J. S. Am. Earth Sci. 14, 693–705.
Pérez, D., Ramos, V., 1996. El Volcanismo de la Región de La Ramada. In: Ramos, V.A., Aguirre-Urreta, M.B., Álvarez, P.P., Cegarra, M.I., Cristallini, E.O., Kay, S.M., Lo Forte, G.L., Pereyra, F.X., Pérez, D.J. (Eds.), Geología de la región del Aconcagua, provincias de San Juan y Mendoza. Subsecretaría de Minería de la Nación. Vol. 24 (9). Dirección Nacional del Servicio Geológico, pp. 275–295.
Pinto, L., Hérail, G., Moine, B., Fontan, F., Charrier, R., Dupré, B., 2004. Using geochemistry to establish the igneous provenances of the Neogene continental sedimentary rocks in the Central Depression and Altiplano, Central Andes. Sediment. Geol. 166 (1/2), 157–183.
Pinto, L., Hérail, G., Montan, F., de Parseval, Ph., 2007. Neogene erosion and uplift of the western edge of the Andean plateau as determined by detrital heavy mineral analysis. Sediment. Geol. 195, 217–237.
Porras, H., Pinto, L., Tunik, M., Giambiagi, L., Deckart, K., 2016. Neogene development of the Alto Tunuyán Basin (33°40′S, Argentina) and its implications for the Andes evolution: insights from petrology, geochemistry and U–Pb LA–ICPMS zircon ages. Tectonophysics 690, 298–317. http://dx.doi.org/10.1016/j.tecto.2016.09.034.
Preston, J., Hartley, A., Mange-Rajetzky, M., Hole, M., May, G., Buck, S., Vaughan, L., 2002. The provenance of Triassic continental sandstones from the Beryl field, northern North Sea: mineralogical, geochemical and sedimentological constraints. J. Sediment. Res. 72, 18–29.
Ramos, V.A., 1999a. Los depósitos sinorogénicos terciarios de la región andina. In: Caminos, R. (Ed.), Geología Argentina. Vol. 29 (22). Instituto de Geología y Recursos Minerales, Buenos Aires, Anales, pp. 651–682.
Ramos, V.A., 1999b. Las provincias geológicas del territorio argentino las provincias geológicas del territorio argentino. In: Caminos, R. (Ed.), Geología Argentina. Vol. 29 (3). Instituto de Geología y Recursos Minerales, Buenos Aires, Anales, pp. 41–96.
Ramos, V.A., Basei, M., 1997. The basement of Chilenia: an exotic continental terrane to Gondwana during the early Paleozoic. In: 8th International Terrane Conference, Proceedings, Terrane Dynamics, Christchurch: New Zealand. Vol. 97. pp. 140–143.
Ramos, V.A., Folguera, A., 2009. Andean flat-slab subduction through time. Geol. Soc. Lond. Spec. Publ. 327 (1), 31–54.
Ramos, V.A., Munizaga, F., Kay, S.M., 1991. El magmatismo Cenozoico a los 33°S de latitud: geocronología y relaciones tectónicas. In: 6th Congreso Geológico Chileno, Santiago, Proceedings, I, pp. 892–896.
Ramos, V., Kay, S., Pérez, D., 1996. El volcanismo de la Región del Aconcagua. In: Ramos, V.A., Aguirre-Urreta, M.B., Álvarez, P.P., Cegarra, M.I., Cristallini, E.O., Kay, S.M., Lo Forte, G.L., Pereyra, F.X., Pérez, D.J. (Eds.), Geología de la región del Aconcagua, provincias de San Juan y Mendoza. Subsecretaría de Minería de la Nación. 24 (14). Dirección Nacional del Servicio Geológico, Anales, pp. 297–316.
Ramos, V.A., Aguirre-Urreta, M.B., Álvarez, P., Cegarra, M.I., Cristallini, E.O., Kay, S.M., Lo Forte, G.L., Pereyra, F.X., Pérez, D.J., 1996. Geología de la Región del Aconcagua, Provincias de San Juan y Mendoza, Subsecretaría de Minería de la Nación, Dirección del Servicio Geológico, Buenos Aires, Anales. 24 (510 pp).
Ramos, V.A., Cristallini, E., Pérez, D.J., 2002. The Pampean flat-slab of the Central Andes. J. S. Am. Earth Sci. 15, 59–78.
Rapela, C.W., Pankhurst, R.J., Casquet, C., Baldo, E., Galindo, C., Fanning, C.M., Dalhquist, J.A., 2010. Grenville-age magmatism of the western Sierras Pampeanas, southern South America: U–Pb SHRIMP dating and tectonic affinities. J. S. Am. Earth Sci. Special Number 29 (1), 105–127. http://dx.doi.org/10.1016/j.jsames.2009.08.004.
Ré, G.H., Jordan, T.E., Kelley, S., 2003. Cronología y paleogeografía del Terciario de la Cuenca Intermontana de Iglesia septentrional, Andes de San Juan, Argentina. Rev. Asoc. Geol. Argent. 58 (1), 31–48.
Reyna, G., Hoke, G.H., Dávila, F.M., 2010. Sedimentation and Exhumation of the Distal Part of the Manantiales Basin: The Chinches Formation, Argentine Precordillera (32° SL). In: 18th International Sedimentology Congress, Proceedings, Mendoza, Argentina, (1 pp).
Rivano, S., Godoy, E., Vergara, M., Villarroel, R., 1990. Redefinición de la Formación Farellones en la Cordillera de los Andes de Chile Central (32°-34°S). Rev. Geol. Chile 17 (2), 205–214.
Rivano, S., Sepúlveda, P., Boric, R., Espiñeira, D., 1993. Hojas Quillota y Portillo, V Región. Servicio Nacional de Geología y Minería, Carta Geológica de Chile, Map N° 73, scale 1:250,000.
Rodríguez, M.P., Pinto Lincoñir, L., Encinas, A., 2012. Neogene erosion and relief evolution in Central Chile forearc (33–34°S) as determined by detrital heavy mineral analysis. Geol. Soc. Am. Spec. Pap. 487, 141–162. http://dx.doi.org/10.1130/2012.2487(09).
Rossel, K., Aguilar, G., Salazar, E., Martinod, J., Carretier, S., Pinto, L., Cabré, A., 2016. Chronology of Chilean Frontal Cordillera building from geochronological, stratigraphic and geomorphological data insights from Miocene intramontane-basin deposits. Basin Res. 1–22. http://dx.doi.org/10.1111/bre.12221.
Ruskin, B.G., Dávila, F.M., Hoke, G.H., Jordan, T.E., Astini, R.A., Alonso, R., 2011. Stable isotope composition of middle Miocene carbonates of the Frontal Cordillera and Sierras Pampeanas: did the Paranaense seaway flood western and central Argentina? Palaeogeogr. Palaeoclimatol. Palaeoecol. 308, 293–303.
Sabeen, H.M., Ramanujam, N., Morton, A., 2002. The provenance of garnet: constraints provided by studies of coastal sediments from southern India. Sediment. Geol. 152, 279–287.
Sato, A.M., Llambías, E.J., Basei, M.A.S., Castro, C.E., 2015. Three stages in the late Paleozoic to Triassic magmatism of southwestern Gondwana, and the relationships with the volcanogenic events in coeval basins. J. S. Am. Earth Sci. 63, 48–69.
Sernageomin, 2003. Mapa geológico de Chile, versión digital, Servicio Nacional de Geología y Minería, 1 Map, scale 1:1,000,000.
Simonetti, A., Shore, M., Bell, K., 1996. Diopside phenocrysts from nephelinite lavas, Napak volcano, eastern Uganda: evidence for magma mixing. Can. Mineral. 34, 411–421.
Stern, D., Wagreich, M., 2013. Provenance of the upper cretaceous to Eocene Gosau group around and beneath the Vienna Basin (Austria and Slovakia). Swiss J. Geosci. 106, 505–527. http://dx.doi.org/10.1007/s00015-013-0150-8.
Strecker, M.R., Hilley, G.E., Bookhagen, B., Sobel, E.R., 2011. Structural, Geomorphic,

and Depositional Characteristics of Contiguous and Broken Foreland Basins: Examples from the Eastern Flanks of the Central Andes in Bolivia and NW Argentina. In: Busby, C., Azor, A. (Eds.), Tectonics of Sedimentary Basins: Recent Advances. John Wiley & Sons, Ltd, Chichester, UK. http://dx.doi.org/10.1002/9781444347166.ch25.

Suriano, J., Mardonez, D., Mahoney, J.B., Mescua, J.F., Giambiagi, L.B., Kimbrough, D., Lossada, A., 2017. Uplift sequence of the Andes at 30°S: insights from sedimentology and U/Pb dating of synorogenic deposits. J. S. Am. Earth Sci. 75, 11–34. http://dx.doi.org/10.1016/j.jsames.2017.01.00.

Varela, R., Basei, M.A.S., González, P.D., Sato, A.M., Naipauer, M., Campos Neto, M., Cingolani, C.A., Meira, T.V., 2011. Accretion of Grenvillian terranes to the west of the Rio de la Plata craton, west of Argentina. Int. J. Earth Sci. 100 (2), 243–272.

Vergés, J., Ramos, V.A., Meigs, A., Cristallini, E., Bettini, F.H., Cortés, J.M., 2007. Crustal wedging triggering recent deformation in the Andean thrust front between 31°S and 33°S: sierras Pampeanas-Precordillera interaction. J. Geophys. Res. 112, 1–22. http://dx.doi.org/10.1029/2006JB004287.

Vicente, J.-C., 2005. La fase primordial de estructuración de la faja plegada y corrida del Aconcagua: importancia de la fase pehuenche del Mioceno inferior. Rev. Asoc. Geol. Argent. 60 (4), 672–684.

von Eynatten, H., Gaupp, R., 1999. Provenance of cretaceous synorogenic sandstones in the eastern Alps: constraints from framework petrography, heavy minerals analysis and mineral chemistry. Sediment. Geol. 124, 81–111.

Walcek, A., Hoke, G., 2012. Surface uplift and erosion of the southernmost argentine Precordillera. Geomorphology 153-154, 156–168. http://dx.doi.org/10.1016/j.geomorph.2012.02.021.

Winocur, D.A., Litvak, V.D., Ramos, V.A., 2015. Magmatic and tectonic evolution of the Oligocene Valle del Cura Basin, main Andes of Argentina and Chile: evidence for generalized extension. Geol. Soc. Lond., Spec. Publ. 399, 109–130. http://dx.doi.org/10.1144/SP399.2.

Yáñez, G.A., Ranero, C.R., von Huene, R., Díaz, J., 2001. Magnetic anomaly interpretation across the southern central Andes (32°-34°S): the role of the Juan Fernandez ridge in the late tertiary evolution of the margin. J. Geophys. Res. 106, 6325–6345.